1 **Development of a New Correction Algorithm Applicable to any Filter-Based Absorption**
2 **Photometer**

3 Hanyang Li[1], Gavin R. McMeeking[2], and Andrew A. May[1]

4 1 The Ohio State University Department of Civil, Environmental, and Geodetic Engineering,
5 Columbus, Ohio, USA

6 2 Handix Scientific, LLC, Boulder, Colorado, USA

7 *Corresponding author*: Andrew A. May (may.561@osu.edu).

8 Abstract

9 Among the various measurement approaches to quantify light absorption coefficient (B_{abs}), filter-
10 based absorption photometers are dominant in monitoring networks around the globe. Numerous
11 correction algorithms have been introduced to minimize the artifacts due to the presence of the
12 filter in these instruments. However, from our recent studies conducted during the Fire Influence
13 on Regional and Global Environments Experiment (FIREX) laboratory campaign, corrected filter-
14 based B_{abs} remains biased high by roughly a factor of 2.5 when compared to a reference value
15 using a photoacoustic instrument for biomass burning emissions. Similar over-estimations of B_{abs}
16 from filter-based instruments exist when implementing the algorithms on six months of ambient
17 data from the Department of Energy (DOE) Atmospheric Radiation Measurement (ARM)
18 Southern Great Plains (SGP) user facility from 2013 (factor of roughly 3). In both datasets, we
19 observed an apparent dependency on single scattering albedo (SSA) and absorption Ångström
20 exponent (AAE) in the agreement between B_{abs} based on existing correction factors and the
21 reference B_{abs}. Consequently, we developed a new correction approach that is applicable to any
22 filter-based absorption photometer that includes light transmission from the filter-based instrument
23 as well as the derived AAE and SSA. For the FIREX and SGP datasets, our algorithm results in
24 good agreement between all corrected filter-based B_{abs} values from different filter-based
25 instruments and the reference (slopes $\approx$ 1 and $R^2 \approx 0.98$ for biomass burning aerosols and slopes
26 $\approx$ 1.05 and $R^2 \approx 0.65$ for ambient aerosols). Moreover, for both the corrected B_{abs} and the derived
27 optical properties (SSA and AAE), our new algorithms work better or at least as well as the two
28 common PSAP-based correction algorithms. The uncertainty of the new correction algorithm is
29 estimated to be ~10%, considering the measurement uncertainties of the operated instruments.
30 Therefore, our correction algorithm is applicable to any filter-based absorption photometer and
31 has the potential to "standardize" reported results across any filter-based instrument.

32 1. Introduction

33 Light-absorbing atmospheric aerosols directly affect the Earth's energy budget by absorbing solar
34 radiation, leading to a warming effect when they are suspended in the atmosphere and to the
35 melting of snow and ice following deposition (Bond and Bergstrom, 2006; Boucher, 2015; Horvath,
36 1993). For decades, scientists have conducted field experiments around the globe to investigate
37 how absorbing aerosols influence the atmospheric radiative balance and interact with clouds (e.g.,
38 Andrews et al. (2011); Cappa et al. (2016); Lack et al. (2008b); Rajesh and Ramachandran (2018);
39 Schwarz et al. (2008)). These experiments may be performed at fixed stations (e.g., observation
40 sites maintained by the Department of Energy (DOE) Atmospheric Radiation Measurement (ARM)
41 program or the National Oceanic and Atmospheric Administration (NOAA) Global Monitoring

42 Division (GMD)) or on mobile platforms (e.g., car trailer, aircraft, and ship), typically involving
43 the measurements of aerosol chemical, physical, and optical properties. Crucial to the
44 quantification of the radiative forcing of absorbing aerosols are measurements of the absorption
45 coefficient (B_{abs}). For example, long-term monitoring of B_{abs} provides essential data to evaluate
46 chemistry-climate model simulations (e.g., Chen et al. (2019); Vignati et al. (2010)), while
47 intensive measurements of B_{abs} during short-term field campaigns allow for the investigation of
48 optical properties that govern features of aerosol forcing (e.g., McMeeking et al. (2014); Olson et
49 al. (2015)).

50 A variety of instruments have been used to measure B_{abs}, which generally classified into two large
51 categories: filter-based techniques and photoacoustic techniques (Lack et al., 2014; Moosmüller
52 et al., 2009). The major difference between the two categories of technique is that B_{abs} is measured
53 after the aerosols are deposited on the filter media in the filter-based instruments, while the aerosols
54 are characterized within an air stream in the photoacoustic instruments. Compared to the filter-
55 based instruments, the photoacoustic instruments have the advantage of avoiding potential artifacts
56 due to the contact of aerosols with filters; therefore, they are often used as the reference instruments
57 in inter-comparison studies of aerosol absorption (e.g., Arnott et al. (2005); Davies et al. (2019);
58 Jiang et al. (2018); Li et al. (2019); Schmid et al. (2006); Sheridan et al. (2005)).

59 Filter-based absorption photometers have been widely used at observational sites around the world
60 due to their ease of operation and relatively low cost. Numerous instruments can be classified as
61 filter-based absorption photometers including the Radiance Research Particle Soot Absorption
62 Photometer (PSAP), the NOAA Continuous Light Absorption Photometer (CLAP), the Brechtel
63 Manufacturing Tricolor Absorption Photometer (TAP), the Magee Scientific Aethalometer
64 (AETH), and the Thermo Scientific Multi-Angle Absorption Photometer (MAAP). Operationally,
65 all of these instruments are similar in that aerosols are deposited onto a filter and the reduction in
66 the transmission (Tr) of light by the particles (sometimes called attenuation (ATN)) is used to infer
67 B_{abs}. Where the instruments may differ is that some are multi-wavelength (multi-λ) instruments
68 (e.g., 3λ-PSAP, CLAP, TAP, 7λ-AETH models), while others are not (e.g., 1λ-PSAP, other AETH
69 models, MAAP).

70 One challenge with filter-based absorption photometers is that biases can arise due to the presence
71 of the filter. For example, light scattering by particles loaded onto the filter or by the filter itself
72 may affect the transmission of light (e.g., (Arnott et al., 2005; Bond et al., 1999)); non-absorbing
73 material may result in absorption enhancement (e.g., (Cappa et al., 2008)); or organic vapors
74 adsorbed to the filter may itself absorb light (e.g., (Subramanian et al., 2007)). Consequently,
75 various correction algorithms exist to minimize these biases, but they are often specific only to
76 certain instruments. For example, some are applicable to the PSAP, CLAP, and TAP (e.g., (Bond
77 et al., 1999; Müller et al., 2014; Ogren, 2010; Virkkula, 2010; Virkkula et al., 2005)), while others
78 are applicable to the AETH (e.g., (Arnott et al., 2005; Collaud Coen et al., 2010; Drinovec et al.,
79 2017; Kirchstetter and Novakov, 2007; Schmid et al., 2006; Virkkula et al., 2007, 2015;
80 Weingartner et al., 2003)).

81 Although the equations associated with these existing correction algorithms are different, they
82 share some commonalities. For example, the filter-based absorption photometers are assessed
83 using laboratory (e.g., ammonium sulfate, fullerene soot) or ambient aerosols during experiments
84 which include reference measurements of B_{abs}. These reference measurements often include either
85 direct photoacoustic B_{abs} or inferred B_{abs} as the difference between the extinction coefficient (B_{ext})

86 and the scattering coefficient (B_{scat}). Correction equations are developed by comparing data
87 between the filter-based instrument and the reference instrument, where the equations often
88 contain one term that accounts for filter loading effects and another that accounts for multiple-
89 scattering effects. Consequently, the correction equations frequently incorporate both Tr and either
90 B_{scat} or the single-scattering albedo (SSA) to account for these effects. However, even when the
91 correction algorithms are applied, potential issues can remain such as:

92 1. Corrected filter-based B_{abs} may remain biased high relative to a reference value of B_{abs} (e.g.,
93   (Arnott et al., 2003; Davies et al., 2019; Lack et al., 2008a; Li et al., 2019; Müller et al., 2011a)).
94 2. Comparisons between the reference instrument and B_{abs} corrected by different algorithms can
95   yield variable agreement (e.g., (Collaud Coen et al., 2010; Davies et al., 2019; Saturno et al.,
96   2017)).
97 3. Corrected B_{abs} from different filter-based absorption photometers may not agree (e.g., (Davies
98   et al., 2019; Müller et al., 2011a)).
99 4. Derived products (such as absorption Ångström exponents (AAE)) may differ based on the
100   implemented correction algorithm (e.g., (Backman et al., 2014; Davies et al., 2019)).
101 5. The agreement between measurements of B_{abs} and estimates of B_{abs} by chemistry-climate
102   models may vary based on the implemented correction algorithm (e.g., (Alvarado et al., 2016)).

103 The first three issues in this list may arise due to differences in aerosol optical properties between
104 those used in deriving the correction equation and those associated with a given aerosol sample,
105 and these issues can propagate through to the fourth issue. The final issue is arguably most
106 important because evaluation of chemistry-climate models may be severely affected by the
107 differences between different correction algorithms, which may inhibit the modeling community
108 from providing accurate projections of future temperature and precipitation response.

109 In this work, we seek to address some of these issues. First, we evaluate the CLAP, TAP, and
110 PSAP using two common PSAP-based correction algorithms, namely Bond et al. (1999) as
111 updated by Ogren (2010) and Virkkula et al. (2005) as updated by Virkkula (2010). For brevity,
112 we refer to these corrections as "B1999" and "V2005" for Bond et al. (1999) and Virkkula et al.
113 (2005), respectively, incorporating their respective updates. In addition, we propose new
114 correction algorithms that are applicable to any filter-based absorption photometer (e.g., CLAP,
115 TAP, PSAP, and AETH) across multiple wavelengths by combining observed filter-based B_{abs}
116 with B_{scat} (e.g., from a co-located nephelometer (NEPH)) and reference B_{abs} (e.g., from a co-
117 located photoacoustic instrument). However, in reality (e.g., at long-term observatories), reference
118 values of B_{abs} are rare, and in some cases, complementary B_{scat} measurements may not exist;
119 consequently, we also provide methods to correct filter-based B_{abs} data in these scenarios. To our
120 knowledge, this is the first study to simultaneously evaluate B1999 and V2005 corrections on
121 PSAP "successors" (i.e., CLAP and TAP) and to present a correction algorithm that is broadly
122 applicable to any filter-based absorption photometer. Regarding the latter, even if our correction
123 algorithm has its own limitations, its use can nevertheless standardize the reporting of B_{abs} in long-
124 term datasets.

125 2. Methodology

126 We developed the general form for our correction algorithms using CLAP and TAP measurements
127 collected from biomass burning (65 fires in total) during the Fire Influence on Regional to Global
128 Environments Experiment (FIREX) laboratory campaign in 2016. By using biomass burning

129   emissions, we considered a dataset spanning a broader range of aerosol optical properties (SSA at
130   652 nm: 0.14-0.98; AAE: 1.25-4.73) than has traditionally been used in developing these
131   correction algorithms. We then conducted further evaluation and validation of the model using
132   ambient data, specifically using CLAP measurements from the DOE ARM Southern Great Plains
133   (SGP) user facility in Lamont, OK, USA (02/01/13 to 07/09/13). Our algorithms were then
134   extended to the AETH data from the FIREX laboratory campaign and the PSAP data collected at
135   the SGP site to verify the generalizability of the algorithms.

136   2.1. The FIREX campaign

137   2.1.1. Experimental setup

138   In October and November of 2016, we participated in the laboratory portion of the FIREX
139   campaign to investigate the wildfire smoke and their impact on the atmosphere. During the
140   campaign, over 100 burns took place at the U.S. Forest Service's combustion facility at the Fire
141   Sciences Laboratory (FSL). The fuels burned in this study are representative of western US
142   ecosystems, such as spruce, fir, various pines, and "chaparral" biome (e.g., manzanita, chamise).
143   (See Koss et al. (2018) and Selimovic et al. (2018) for more details).

144   A typical burn lasted for 1-3 hours depending on the smoke sampling strategies (e.g., stack burns
145   versus room burns). During each burn, one or multiple "snapshots" of smoke (typical B_{abs} at 652
146   nm ranged from 100 to 1200 Mm^{-1}) were transferred from the combustion room at FSL into a
147   mixing chamber (210 L) through a long transfer duct (30 m in length, 8" in diameter). The smoke
148   was then diluted by filter air (~230 LPM) in the chamber. Once the concentration in the chamber
149   was stable (detected by the Photoacoustic Extinctiometer (PAX) which was operated continuously
150   through all fires), the smoke was passed to a suite of instruments to obtain aerosol and gas phase
151   parameters. This chamber also served as an intermediate between the transfer duct and the
152   instrumentation to minimize potential biases that arose due to different sample flow rates and
153   sample locations of the instruments. A more detailed description of our experiments can be found
154   in Li et al. (2019).

155   2.1.2. Measurements of aerosol optical properties

156   During the campaign, five instruments provided measurements of B_{abs} (CLAP, NOAA GMD; TAP,
157   Brechtel Manufacturing Inc. (BMI); Aethalometer (Model AETH-31), Magee Scientific; and two
158   PAXs (Model PAX-870 and PAX-405), Droplet Measurement Technologies) and two instruments
159   provided measurements of B_{scat} (PAX-870 and PAX-405). The instruments included in the present
160   work are summarized in Table 1.

161   Both CLAP and TAP provide B_{abs} measurements of the particles deposited on a filter, similar to
162   PSAP. Different from PSAP, there are multiple filter spots (8 sample spots and 2 reference spots)
163   cycling of one filter in CLAP and TAP, enabling the instruments to run continuously through two
164   or three burns without changing filter. In the CLAP and TAP, sample illumination is provided by
165   LEDs operated at three wavelengths (467, 528, and 652 nm). Here, we apply both B1999 and
166   V2005 to CLAP and TAP data, similar to previous work (e.g., (Backman et al., 2014; Davies et
167   al., 2019)).

168   The key differences between the CLAP and TAP during the FIREX campaign include:

169   1. The spot change of the CLAP was manually performed when Tr reached approximately 0.5
170   (or ATN decreased to ~69), while the TAP advanced to a new spot automatically with a Tr
171   threshold set to be 0.5.
172   2. The spot area, flow rate, and LED-detected wavelengths differed slightly (Table 1).
173   3. The CLAP recorded B_{abs} every one minute, while the TAP recorded B_{abs} every ten seconds. To
174   enable the following analysis, we compute the 1-minute averages of TAP-derived parameters.
175   4. For the first portion of the campaign (the first 17 days of the 45-day campaign), Pallflex E70-
176   2075S filters were used in the CLAP while Azumi filters (model 371M, Azumi Filter Paper
177   Co., Japan) were used in the second portion of the campaign (due to a lack of availability of
178   the Pallflex filters). The TAP was equipped exclusively with the Azumi filters throughout the
179   campaign. We apply the filter correction recommended in Ogren et al. (2017) to the CLAP and
180   convert from Pallflex to Azumi filters.
181   5. BMI substantially re-engineered the CLAP in their development of the TAP.

182 These differences resulted in variable agreement between the CLAP and TAP during FIREX;
183 however, the two instruments did largely agree within experimental uncertainty (e.g., see Fig. S8
184 and Fig. S13 in Li et al. (2019)).

185 A PAX measures B_{abs} and B_{scat} simultaneously for suspended particles using a modulated diode
186 laser. We use these photoacoustic absorption measurements as the reference to evaluate the filter-
187 based B_{abs} and develop our correction algorithms. To enable the evaluation of CLAP and TAP
188 which operate at different wavelengths than the PAXs, we interpolate the measurements of B_{abs}
189 and B_{scat} to the wavelengths of 467, 528, and 652 nm using the values of AAE and scattering
190 Ångström exponents (SAE), similar to Backman et al. (2014) and Virkkula et al. (2005).
191 Theoretically, AAE and SAE fit absorption and scattering as power law functions of wavelength
192 (Bergstrom et al., 2007).

193 Due to the numerous correction algorithms for the Aethalometer (e.g. (Arnott et al., 2005; Collaud
194 Coen et al., 2010; Kirchstetter and Novakov, 2007; Saturno et al., 2017; Schmid et al., 2006;
195 Virkkula et al., 2007; Weingartner et al., 2003)), we do not evaluate these in the present work to
196 limit the scope. In fact, the majority of our focus is the B1999 and V2005 corrections to TAP and
197 CLAP. However, we still test the performance of the new algorithms on the AETH to explore its
198 applicability to that instrument.

199 2.2. Measurements of aerosol optical properties at the SGP observatory

200 The ambient data used in this manuscript are the ground-based aerosol data measured at the SGP
201 observatory from 02/01/13 to 07/09/13 (archived at https://www.archive.arm.gov/discovery/). For
202 evaluation purposes, we randomly select a range of dates during which the observations are valid
203 (without incorrect, suspect, and missing data) and the PASS is operated after laser (532 nm)
204 upgrade.

205 At the site, an impactor was used to switch the sampling between two cutoffs (particle diameter
206 <10 μm (PM10) in the first 30 minutes of each hour and <1 μm (PM1) in the latter 30 minutes of
207 each hour). The aerosols exiting from the impactor were dried to RH less than 40% and passed to
208 a CLAP, a PSAP, and two NEPHs. Moreover, a three-wavelength photoacoustic soot spectrometer
209 (PASS-3) was operated at the site and measured B_{abs} and B_{scat} of the aerosols, but these aerosols
210 did not pass through the impactor (e.g., characterizing total suspended particles (TSP)). Typical
211 B_{abs} and B_{scat} reported at the site ranged from 0 to 10 Mm^{-1} and 0 to 50 Mm^{-1} at 550 nm, respectively

212   (e.g., (Sherman et al., 2015)). Although the site is rural (clean background air), long-term transport
213   aerosols (such as mineral dust, absorbing organic aerosols, and secondary organic aerosols (SOA))
214   may affect the local aerosol properties (Andrews et al., 2019).

215   We preprocess the SGP data in three steps. First, due to the systematic difference of aerosol sizes
216   between PASS-derived and filter-based absorption, we only include the PM10 observations,
217   inherently assuming that any differences in the optical properties of PM10 and TSP are negligible.
218   Then, we smooth the 1-second data into 10-minute averages. Thirdly, we estimate the detection
219   limits at each of the three wavelengths in the PASS-3 using the data measured during the
220   "background zero" periods (Allan, 1966) and discard the observations which are below the
221   detection limits. With a 10-min-averaging-time, the detection limits (3σ) for the PASS-3 are 0.78
222   Mm^{-1} (405 nm), 2.01 Mm^{-1} (532 nm), and 0.30 Mm^{-1} (781 nm). For the filter-based instruments,
223   the detection limits are based on previous studies (See Table 1). Moreover, we only retain the
224   observations that satisfy B_{abs} (405 nm) > B_{abs} (532 nm) > B_{abs} (781 nm) (or AAE>0), similar to
225   Fischer and Smith (2018). As with the PAX data from the laboratory, we adjust the PASS-derived
226   B_{abs} to 467, 528, and 652 nm using the inferred AAE values for each 10-minute average.

227 **Table 1** Summary of specifications for instruments relevant to this work.

Instrument	Flow rate (LPM)	Spot area (cm²)	Type of filter	Measured parameters	Response time	Measurement uncertainty	Detection limit (3σ, Mm⁻¹)
PAX-870	1.0	-	-	B_{abs} and B_{scat} (870 nm)	1s	~11% (B_{abs}) ~17% (B_{scat}) (Nakayama et al., 2015)	0.47 (B_{abs}) 0.66 (B_{scat}) [a]
PAX-405	1.0	-	-	B_{abs} and B_{scat} (405 nm)	1s	4% (B_{abs}) 7% (B_{scat}) (Nakayama et al., 2015)	0.27 (B_{abs}) 0.60 (B_{scat}) [a]
PASS-3 [b]	1.0	-	-	B_{abs} and B_{scat} (405, 532, and 781 nm)	1s	4 %, 8 %, and 11 % (B_{abs}) (Nakayama et al., 2015)	0.78 (405 nm) 2.01 (532 nm) 0.30 (781 nm) [a]
NEPH [b]	7.5	-	-	B_{scat} (450, 550, and 700 nm)	1s	10% (Anderson et al., 1996)	0.29 (450 nm) 0.11 (550 nm) 0.17 (700 nm) (5-min average) (Müller et al., 2011b)
CLAP	0.83 ± 0.02 (FIREX) 0.945 (SGP)	0.199 (FIREX) 0.195 (SGP)	Pallflex E70-2075S and Azumi filter (model 371M) [c]	B_{ATN} and Tr [d] (467, 529, and 653 nm)	60s	30% (Ogren et al., 2017)	0.6 (1-min average), 0.12 (10-min average) (Ogren et al., 2017)
TAP	1.26 ± 0.01	0.253	Azumi filter (model 371M) [c]	B_{ATN} and Tr [d] (467, 528, and 652 nm)	10s	30% (Laing et al., 2016)	2.67 (467 nm) 4.11 (528 nm) 2.13 (652 nm) (30-s average) (Davies et al., 2019)
AETH	2.4	0.5	quartz fiber sampling tape	B_{ATN} and Tr (370, 470, 520, 590, 660, 880, and 950 nm)	120s	10% (Sedlacek, 2016)	0.1 (Sedlacek, 2016)
PSAP	1.0	0.178	Pallflex E70-2075W	B_{ATN} and Tr [d] (470, 522, and 660 nm)	60s	~15% (Bond et al., 1999)	0.3 (Springston, 2016)

228 [a] The detection limits of PAX and PASS-3 are determined by Allan deviation analysis (Allan, 1966) of B_{abs} during "background zero".

229 [b] During the analysis of the data collected at the SGP, we use B_{abs} derived by the PASS and B_{scat} derived by the NEPH to yield the coefficients in the algorithms.

230 [c] Two types of filters were used during the FIREX campaign (See Sect. 2.1.2).

231 [d] The operating wavelengths of CLAP, TAP, and PSAP are stated slightly different by the instrument manufactures. We simply use 467, 528, and 652 nm throughout

232 this manuscript.

2.3. Calibrations

Following Bond et al. (1999) and Ogren et al. (2010), the filter-based instruments were calibrated and corrected for sample area, flow rate, and filter type (see Li et al. (2019) for the FIREX data and Sherman et al. (2015) for the SGP data). Other than that, we did not do any verification beyond the manufacturer's calibration for the filter-based instruments. The SGP nephelometer measurements were corrected for truncation effects (Sherman et al., 2015). The FIREX photoacoustic measurements were calibrated by ammonium sulfate aerosol and fullerene soot (Li et al., 2019).

2.4. The correction algorithms

In filter-based instruments, the light intensities transmitted through the sample spot and blank spot of the filter are recorded as I_s and I_b, respectively. The logarithmic ratio of the two intensities at time t is defined as ATN using the Beer-Lambert law:

$$ATN(t) = -100 \times ln\frac{I_s(t)}{I_b(t)}$$

where ATN = 0 when beginning a new filter spot (t = 0).

The ATN can be related to Tr by normalizing I_s/I_b at time t relative to I_s/I_b at the start of a new filter spot (t = 0):

$$Tr(t) = \frac{I_s(t)/I_b(t)}{I_s(0)/I_b(0)} = exp(\frac{-ATN(t)}{100})$$

The change of ATN over a time interval (Δt) for the instrument operated at a volume flow rate of Q and spot area of A yields the attenuation coefficient (B_{ATN}) for that time interval:

$$B_{ATN} = \frac{A}{Q \times \Delta t} \times \Delta ATN$$

B_{ATN} is finally converted to B_{abs} by applying correction algorithms. The general form of the correction algorithms presented for the PSAP in Bond et al. (1999) and Virkkula et al. (2005) can be summarized as:

$$B_{abs} = B_{ATN} \times f(Tr) - C_1 \times B_{scat}$$

where f(Tr) is some function of Tr (that may vary between approaches), correcting for the filter loading effect. C_1 is a constant that may vary with wavelength; specifically, it is a penalty for the light scattering by the particles collected on the filter which may contribute to the quantification of ATN. In most atmospheric and laboratory studies, B_{scat} is measured independently, typically using a co-located NEPH.

Besides the above mentioned B1999 and V2005 corrections, the constrained two-stream (CTS) correction proposed by Müller et al. (2014) can be also applied on PSAP-similar instruments. The CTS correction was developed based on the relationship between absorption optical depth and B_{abs}. However, it is not straightforward to reformulate the CTS correction as a function of Tr as those presented in Eq. (5) and Eq. (6). Thus, we exclude the B_{abs} results corrected by the CTS correction in the following analysis. For those who are interested in the B_{abs} results corrected by the CTS correction, we provide the correction results of our SGP-CLAP data in Fig. S9.

269 2.4.1. The B1999 correction

270 Bond et al. (1999) was the first study to present the correction algorithm for filter-based
271 instruments. This empirical correction was originally developed for the PSAP operated at 550 nm
272 using various mixtures of laboratory-generated nigrosin (SSA $\approx$ 0.5) and ammonium sulfate (SSA
273 $\approx$ 1) with B_{abs} ranged from 0 to 800 Mm^{-1}.

274 After calibrating the flow rate and spot area of the PSAP, Bond et al. (1999) derived $C_1 = 0.016$
275 and defined f(Tr) as follows:

276 $$f(Tr)_{B1999} = \frac{1}{C_2 \times Tr + C_3}$$ 5

277 Following an adjustment by Ogren (2010), C_2 and C_3 in Eq. (5) were updated to 1.55 and 1.02,
278 respectively. These are the values used in the present work (Table 2) for B1999. Moreover, Ogren
279 (2010) stated that the correction forms of Eq. (4) and Eq. (5) were valid for any wavelength, while
280 additional experiments were needed to establish the equation parameters for the wavelengths other
281 than 574 nm.

282 2.4.2. The V2005 correction

283 Virkkula et al. (2005) developed a correction algorithm for both three-wavelength PSAP (467, 530,
284 and 660 nm) and one-wavelength PSAP (574 nm) using the same functional form as Eq. (4). Since
285 the operating wavelengths of the photoacoustic instruments and the NEPH were different from
286 those of the PSAP, the measured photoacoustic B_{abs} and B_{scat} was extrapolated or interpolated to
287 467, 530, and 660 nm, using inferred AAE and SAE respectively. In this study, the authors used
288 various mixtures of kerosene soot, ammonium sulfate, and polystyrene latex (SSA ranged from
289 0.2 to 0.9) with B_{abs} ranging from 0 to 800 Mm^{-1} at 530 nm.

290 Different from the f(Tr) in the B1999 correction which was a reciprocal function of Tr, the f(Tr)
291 presented in V2005 was a multivariate linear function of the natural logarithm of Tr and SSA
292 (including an interaction term between the two):

293 $$f(Tr(\lambda), SSA(\lambda))_{V2005} = C_4 + C_5 \times (C_6 + C_7 \times SSA(\lambda)) \times ln(Tr(\lambda))$$ 6

294 where the parameters in Eq. (6) vary with wavelengths. The parameters in V2005 were updated in
295 Virkkula (2010) by correcting for flowmeter calibration (Table 2).

296 Due to the unknown values of SSA before deriving B_{abs}, Virkkula et al. (2005) provided a solution
297 through an iterative procedure. In the iteration, B_{abs} is first calculated using the B1999 correction
298 (e.g., Eq. (4) and Eq. (5)) and is then used to compute the initial guess of SSA for use in Eq. (6).
299 The B_{abs} and SSA can be updated using Eq. (4) and Eq. (6) until convergence is reached.

300 2.4.3. Refitting the coefficients in B1999 and V2005

301 With the reference measurements of B_{abs} from the photoacoustic instruments, we are able to refit
302 the coefficients in the B1999 and V2005 corrections (C_2 to C_7 in Eq. (5) and Eq. (6)) using our
303 data. Specifically, we use the Levenberg-Marquardt algorithm (1944) to iteratively fit the
304 coefficients until the chi-square of the coefficients are minimized. The fitting is implemented using
305 the "Curvefit" function in Igor Pro. It is worth noting that the derived coefficients may only be
306 valid for the SGP and FIREX data. For aerosol properties different from our study, the optimal
307 coefficients are likely to be different from the ones reported here. Hereafter, the B1999 and V2005

308 results with refitted coefficients are referred to as "updated B1999" and "updated V2005",
309 respectively.

310 2.4.4. The new correction

311 We develop a set of new correction algorithms with the same general form as Eq. (4) using the
312 biomass burning emissions from 65 different burns during the FIREX laboratory study, providing
313 a broader range of aerosol optical properties and aerosol concentrations than previous work. This
314 was motivated by the disagreement that remained between filter-based and photoacoustic
315 instruments, even after applying B1999 to the data (e.g., see Li et al. (2019) Fig. 4 and our Fig. 2
316 below). These differences may persist because we were effectively extrapolating the B1999
317 correction equation to values outside the range for which it was developed.

318 This new correction is developed based on multiple linear regression techniques with three
319 dependent variables of ln(Tr), SSA, and AAE and one independent variable of B_{abs}/B_{ATN} (Eq. (7)
320 – (9)). As with other correction equations, this model takes into account the influence of scattering
321 and weakly-absorbing materials, but we have the additional aim of developing a model that is
322 applicable to any filter-based absorption photometer.

323 Similar to the B1999 and V2005 corrections, this new model starts with the general form of Eq.
324 (4), re-written here to define B_{scat} in terms of SSA and B_{abs}.

$$B_{abs}(\lambda) = B_{ATN}(\lambda) \times f(Tr(\lambda)) - C_1 \times \frac{SSA(\lambda)}{1-SSA(\lambda)} \times B_{abs}(\lambda) \qquad 7$$

326 Re-arranging this equation to move all B_{abs} terms to the left-hand side yields:

$$B_{abs}(\lambda) = B_{atn}(\lambda) \times g(Tr(\lambda), SSA(\lambda)) \qquad 8$$

328 where $g(Tr(\lambda), SSA(\lambda)) = f(Tr(\lambda)) \times \frac{1-SSA(\lambda)}{1-(1-C_1)\times SSA(\lambda)}$.

329 We define a new function "g" that can be used in Eq. (8). Specifically, we construct a multivariate
330 linear model for "g", introducing AAE as a dependent variable and including interaction terms
331 between SSA, AAE, and ln(Tr):

332 $g(Tr(\lambda), SSA(\lambda), AAE) = G_0 + G_1 \times ln(Tr(\lambda)) + G_2 \times SSA(\lambda) + G_3 \times AAE + G_4 \times ln(Tr(\lambda)) \times SSA(\lambda) +$

333 $\qquad\qquad G_5 \times SSA(\lambda) \times AAE + G_6 \times ln(Tr) \times AAE + G_7 \times SSA(\lambda) \times AAE \times ln(Tr(\lambda)) \qquad 9$

334 Equation (9) suggests that different combinations of SSA, AAE and ln(Tr) can result in the same
335 value of "g" (i.e., B_{abs}/B_{ATN}); likewise, a given value of B_{abs}/B_{ATN} may have infinitely many points
336 with distinct slopes passing through it (Fig. S3). Although Eq. (9) is developed based on statistical
337 approaches, we attempt to relate this statistical model to physical effects. The coefficients $G_1 - G_3$
338 are fairly straightforward, as these account for the influence of filter loading (G_1), relative light
339 scattering by the aerosols (G_2), and the brownness of the aerosols (G_3). The interaction terms (G_4
340 – G_7) are more difficult in assigning a physical meaning; however, the interaction between filter
341 loading and relative light scattering (G_4) is might be interpreted as an absolute light scattering by
342 the aerosols on the filter, while the interaction between filter loading and aerosol brownness (G_6)
343 is somewhat analogous to G_4. The three-way interaction between filter loading, scattering and
344 brownness of aerosols (G_7) is required because of the three two-way interaction terms.

345 To further this physical interpretation of our statistical model (Eq. 9), we explore the relationship

346 between $\frac{B_{abs}}{B_{ATN}}$ and ln(Tr), which essentially follows a "y = m·x + b" form, where y is $\frac{B_{abs}}{B_{ATN}}$ and x is

347 ln(Tr). The slope (m) is defined as $G_1 + G_4 \times SSA + G_6 \times AAE + G_7 \times SSA \times AAE$, and the intercept

348 (b) is defined as $G_2 \times SSA + G_3 \times AAE + G_5 \times SSA \times AAE$. Therefore, different combinations of SSA

349 and AAE modulate this relationship between $\frac{B_{abs}}{B_{ATN}}$ and ln(Tr). For example, loading "black"

350 particles on the filter (e.g., AAE ~1 and SSA ~0.3) tends to produce larger values of $\frac{B_{abs}}{B_{ATN}}$, while

351 loading "white" particles on the filter (e.g., AAE ~3 and SSA ~0.9) tends to produce smaller values

352 of $\frac{B_{abs}}{B_{ATN}}$ (see Fig. S3 of this work and Fig. 4 in Virkkula et al.(2005)). This relationship becomes

353 more complex when considering, e.g., mixed sulfate and black carbon particles; SSA can be high

354 while AAE is low, and the corresponding $\frac{B_{abs}}{B_{ATN}}$ can be variable (also see Fig. S3). Therefore, in

355 order to properly compensate for the effects of loading and aerosol optical properties, a multiple

356 linear regression with interaction terms is introduced in Eq. (9).

357 A detailed description of the procedure for the model development (e.g., variable transformation

358 (from Tr to ln(Tr)), variable selection using best-subsets and stepwise approaches, and model

359 assessment) is provided in the Supplementary Material. We evaluate the model by plotting $\frac{B_{abs}}{B_{ATN}}$

360 against aerosol properties not included in Eq. (9) (such as relative humidity and aerosol geometric

361 mean diameter, which have been previously reported to bias corrections of filter-based B_{abs},

362 (Moteki et al., 2010; Nakayama et al., 2010; Schmid et al., 2006)). The results are presented in Fig.

363 S5-S7.

364 As in V2005, iteration is required in our algorithm because B_{abs} is dependent on knowledge of

365 SSA and AAE, which themselves are dependent on B_{abs}. We propose the following iterative

366 process to update SSA and AAE in the model.

367 1. Initialize AAE from B_{ATN} across the three wavelengths ($B_{ATN} \sim \lambda^{-AAE}$) and initialize SSA for

368   each wavelength using B_{ATN} from the filter-based absorption photometer and B_{scat} from a co-

369   located NEPH, i.e., $SSA(\lambda) = \frac{B_{scat}(\lambda)}{B_{scat}(\lambda) + B_{ATN}(\lambda)}$.

370 2. Yield an initial set of coefficients G_0 through G_7 for each wavelength to calculate g(Tr, SSA,

371   AAE) in Eq. (9), using one of the Algorithms described in Sect. 2.5.

372 3. Calculate B_{abs} for each wavelength using Eq. (8).

373 4. Update AAE and SSA using B_{abs} calculated in Step 3.

374 5. Derive a new set of coefficient values.

375 6. Iterate Steps 3-5 until converged.

Table 2 Overview of the studies of B1999 and V2005 and the description of our experiments.

Study	Aerosol source	SSA subset	Range of B_{abs} (Mm^{-1})	Filter-based instrument for B_{abs}	Reference instrument for B_{abs} [a]	Instrument for B_{scat} [a]	Coefficient values in the correction algorithm [b, c]		
The study in **B1999**	Lab-generated aerosols, including various mixtures of nigrosin and ammonium sulfate	0.5-1 (550 nm)	0-800 (550 nm)	One-λ PSAP (550 nm)	The difference between extinction (OEC) and scattering coefficient (NEPH) [d]	NEPH (450, 550, and 700 nm)	$C_1 = 0.016 \pm 0.023$ (550 nm) $C_2 = 1.55 \pm 0.25$ (550 nm) $C_3 = 1.02 \pm 0.17$ (550 nm)		
The laboratory study in **V2005**	Lab-generated aerosols, including various mixtures of kerosene soot, ammonium sulfate, and polystyrene latex	0.2-0.9 (530 nm)	0-800 (530 nm)	One-λ PSAP (550 nm), three-λ PSAP (467, 530, 660 nm)	The average of the PA (532 nm and 1064 nm) and the difference between extinction (OEC) and scattering coefficient (NEPH) [d]	NEPH (450, 550, and 700 nm)	**467 nm** $C_1 = 0.015$ $C_4 = 0.377 \pm 0.013$ $C_5 = -0.640 \pm 0.007$ $C_6 = 1.16 \pm 0.05$ $C_7 = -0.63 \pm 0.09$	**530 nm** $C_1 = 0.017$ $C_4 = 0.358 \pm 0.011$ $C_5 = -0.640 \pm 0.007$ $C_6 = 1.17 \pm 0.03$ $C_7 = -0.71 \pm 0.05$	**660 nm** $C_1 = 0.022$ $C_4 = 0.352 \pm 0.013$ $C_5 = -0.674 \pm 0.006$ $C_6 = 1.14 \pm 0.11$ $C_7 = -0.72 \pm 0.16$
The ambient study in **V2005**	Ambient aerosols measured during RAOS and NEAQS [e]	0.75-1 (530 nm)	0-15 (530 nm)	One-λ PSAP (550 nm), three-λ PSAP (467, 530, 660 nm)	PA (532 nm and 1064 nm)	NEPH (450, 550, and 700 nm)			
FIREX [f]	Biomass burning aerosols under relatively controlled laboratory conditions	0.2 -1 (550 nm)	38-1800 (550 nm)	CLAP (467, 529, 652 nm), TAP (467, 528, 653 nm), AETH (370, 470, 520, 590, 660, 880, 950 nm)	PAX (405 nm and 870 nm)	PAX (405 nm and 870 nm)	See Table 4 and Tables S6-S10		
SGP (02/01/13 to 07/09/13) [f, g]	Ambient aerosols collected at the SGP user facility in Lamont, OK	0.75-1 (530 nm)	0-8 (550 nm)	CLAP (461, 522, 653 nm), PSAP (470, 522, 660 nm)	PASS (405, 532, and 781 nm)	NEPH (450, 550, and 700 nm)			

[a] The operating wavelengths are based on the manufacturer specifications.

[b] The coefficients provided in Table 2 are the values presented in Ogren (2010) and Virkkula (2010), which are updated from Bond et al. (1999) and Virkkula et al. (2005), respectively.

[c] We reformulate the correction equations in the original publications to agree with Eq. (4)–(6) in this manuscript. C_1 to C_7 are the coefficients in the present work.

[d] OEC is optical extinction cell and PA is the instrument using photoacoustic technique.

[e] RAOS and NEAQS are Reno Aerosol Optics Study and New England Air Quality Study, respectively.

[f] The relative humidity (%) of the sampled aerosols from the FIREX and SGP study is 29.3 ± 3.3 and 26.1 ± 13.94, respectively.

[g] The scatterplot of AAE and SAE for the SGP data can be found in Fig. S15. Our results of AAE and SAE are compared to the values reported for different NOAA Earth System Research Laboratory (ESRL) observational sites in Schmeisser et al. (2017).

2.5. Application of correction algorithms

In developing a procedure for applying our algorithm, we envision three potential scenarios:

1. Algorithm A: The filter-based instrument is co-located with a NEPH and reference instrument providing B_{abs}. This scenario facilitates the computation of G_0 through G_7 in Eq. (9) (step 2 in the iterative process) as well as the derivation of new coefficients for existing correction algorithms. This scenario can also enable the develop of a new a set of coefficients that may be more appropriate for aerosol sources that we do not consider here.
2. Algorithm B: The filter-based instrument is co-located with a NEPH but not a reference instrument providing B_{abs}, which is perhaps the most likely scenario (at least at many long-term monitoring sites). This scenario requires an initial guess of the coefficients; we provide sets of these in Table 4 below for different filter-based instruments and aerosol sources.
3. Algorithm C: The filter-based instrument is deployed with neither a co-located NEPH nor a reference instrument providing B_{abs}. This scenario is the most challenging, because there are no measurements of B_{scat} to compute SSA; to address this issue, we propose the use of a non-linear relationship between SSA and AAE (AAE = $a + b \times SSA^c$) to provide an initial guess of SSA in the iterations.

To aid in decision-making between algorithms, we developed a flow chart for selecting appropriate correction algorithm for CLAP, TAP, and PSAP (Fig. 1). Furthermore, Igor Pro (WaveMetrics, Inc.) and Python (Version 3.7.5) based program for selecting and implementing our correction algorithms can be found at https://doi.org/10.5281/zenodo.3742342.
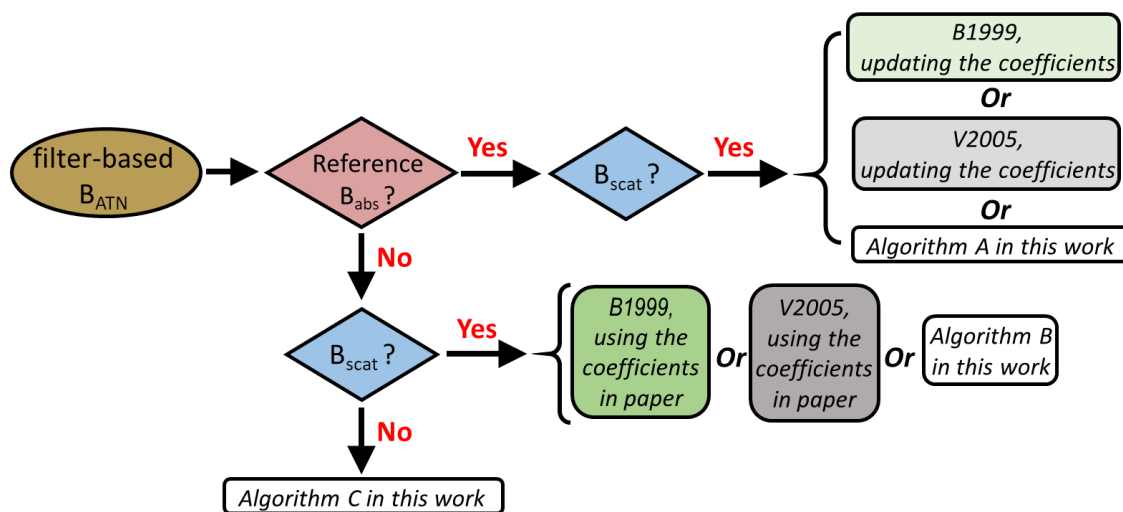
Figure 1. The flow-chart for the application of correction algorithms on PSAP, CLAP, and TAP. Similar logic is followed for the AETH.

3. Results and discussion

3.1. Application of the previous algorithms on different aerosols

We first consider the application of the B1999 and V2005 corrections on different combinations of aerosol type and filter-based absorption photometer. Specifically, we apply the two corrections to the biomass burning data from the FIREX laboratory campaign (CLAP and TAP) as well as six

months of ambient data from the SGP site (CLAP and PSAP). In doing so, we use the "default" coefficients recommended in B1999 and V2005 as well as "updated" coefficients that are estimated via regression techniques. It is important to keep in mind that the updated coefficient values of B1999 and V2005 (Table S7) are only valid for the aerosols investigated in this study. Future experiments are needed to systematically determine how the coefficients in B1999 and V2005 may change for different aerosol types. We focus on the results of the CLAP in the main text, because a CLAP is the only instrument common to deployments for both FIREX and SGP. The results of the TAP from FIREX and the PSAP from the SGP site can be found in the Supplementary Material (Table S5 and Fig. S11).

Our inter-comparison between the corrected CLAP-derived B_{abs} and reference B_{abs} for the FIREX and SGP data is provided in Fig. 2 and Table 3. For the FIREX measurements, both analyses (using the "default" coefficients and updating the coefficients) suggest good correlation (coefficient of determination (R^2) > 0.9) between the CLAP and the reference across all three wavelengths. Nevertheless, the corrections using the "default" coefficients result in over-prediction of B_{abs} by factors of ~2.5. If we update the coefficients in the corrections, there is an obvious improvement in the agreement (i.e., slope $\approx$ 1; R^2 increases). The results are generally similar for SGP, although the R^2 for ambient data is generally lower for ambient data (R^2 < 0.7). Decreased R^2 may be due to the lower aerosol concentrations measured in ambient air, which could lead to lower signal-to-noise in the instruments. Moreover, it is worth mentioning that for both datasets (FIREX and SGP), the corrected B_{abs} from different filter-based absorption photometers using the "default" approaches does not agree with each other (slopes range from 0.69 to 1.40). However, after updating the coefficients, the slopes approach unity (Table S6).

436
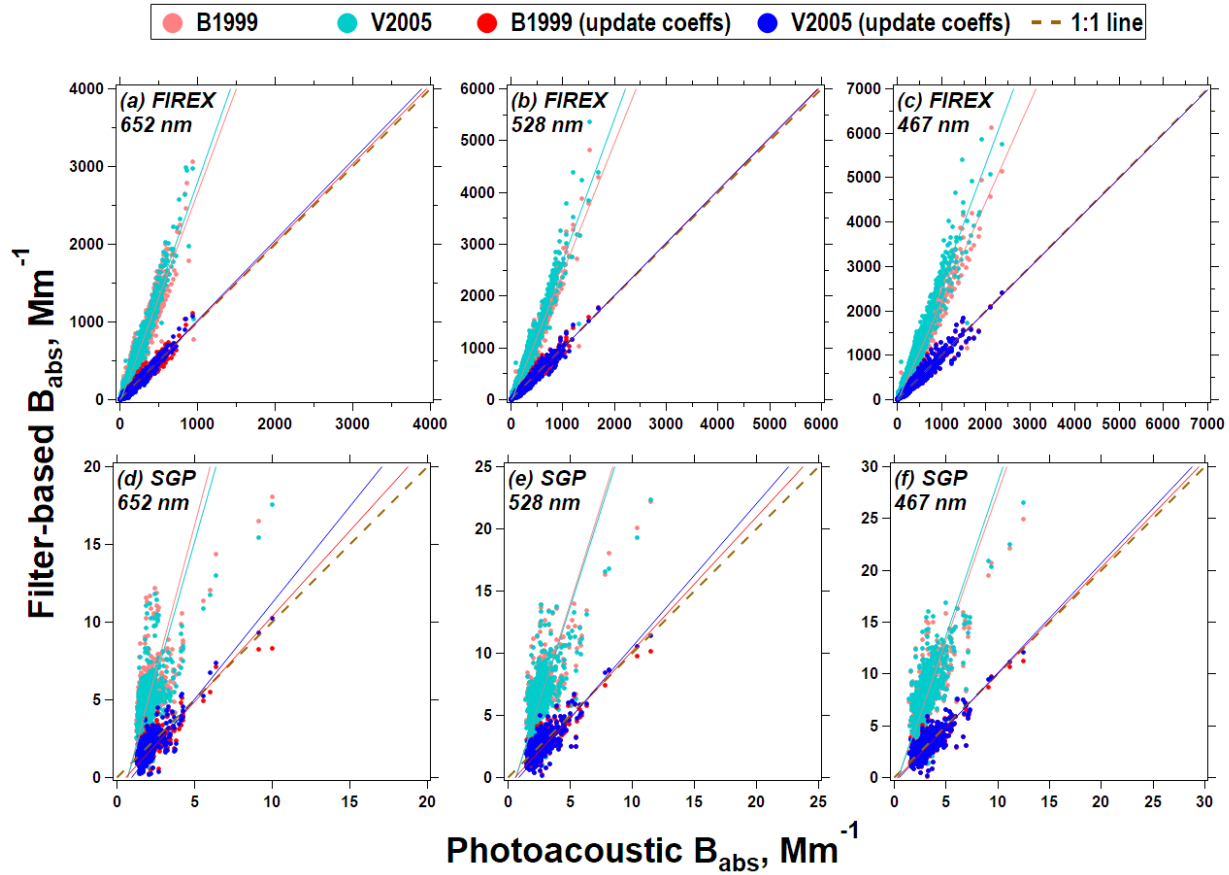
Figure 2. Inter-comparison between the CLAP-derived B_{abs} corrected by the B1999 and V2005 algorithms and the reference B_{abs} at 652, 528, and 467 nm for both FIREX and SGP data. The solid lines represent linear regressions, while the dashed line is a 1:1 line.

Table 3 Relationship between the CLAP-derived B_{abs} corrected by the B1999 and V2005 algorithms (including updated coefficients) and the reference B_{abs} at 652, 528, and 467 nm. The relationship is achieved using major axis regression (Ayers, 2001). The value in parentheses represents the coefficient of determination (R^2) of the linear relationship.

		652 nm	528 nm	467 nm
FIREX	**B1999**	y = -39 + 2.69x (0.94)	y = -49 + 2.50x (0.96)	y = -45 + 2.26x (0.97)
	V2005	y = -46 + 2.83x (0.96)	y = -57 + 2.75x (0.96)	y = -56 + 2.68x (0.96)
	B1999 (update coeffs)	y = -8.4 + 1.02x (0.96)	y = -7.7 + 1.01x (0.97)	y = -3.4 + 1.00x (0.96)
	V2005 (update coeffs)	y = -9.4 + 1.03x (0.97)	y = -7.3 + 1.01x (0.97)	y = -3.0 + 1.00x (0.96)
SGP	**B1999**	y = -2.60 + 3.77x (0.41)	y = -1.90 + 3.20x (0.49)	y = -0.98 + 2.85x (0.55)
	V2005	y = -2.50 + 3.54x (0.41)	y = -2.00 + 3.15x (0.48)	y = -1.10 + 2.96x (0.55)
	B1999 (update coeffs)	y = -0.29 + 1.10x (0.60)	y = -0.29 + 1.08x (0.63)	y = -0.17 + 1.03x (0.65)
	V2005 (update coeffs)	y = -0.57 + 1.24x (0.65)	y = -0.50 + 1.15x (0.67)	y = -0.27 + 1.06x (0.67)

444

In the FIREX data, there is an apparent dependency of the updated coefficients on the wavelength of light, but more importantly, on the aerosol optical properties, namely SSA and AAE (Tables S7-S9). However, in the ambient data from SGP, the dependency on optical properties is less

448   obvious (Tables S10-S11). Nevertheless, all of these coefficients differ from those reported in
449   B1999 and V2005 (again, derived for the PSAP rather than the CLAP), which highlights the
450   potential need to use coefficient values that are appropriate for the instrument being used, its
451   wavelength(s) of light, and optical properties that are representative of the sampled aerosols when
452   applying correction factors to B_{ATN}.

453   3.2. Application of the new algorithms to the FIREX data

454   The co-location of the CLAP, TAP, AETH, and PAX during FIREX allows us to apply each
455   algorithm (A, B, C) to these data. Similar to Sect. 3.1, we focus our discussion on the CLAP with
456   details on the TAP and AETH presented in the Supplementary Material (Fig. S11-S12). However,
457   we provide the recommended initial guesses in the new algorithms and the comparison of
458   absorption (corrected filter-based B_{abs} versus reference B_{abs}) for all filter-based absorption
459   photometers in Table 4 and Table 5 to help readers quickly retrieve key information of our
460   algorithms.

461   Figure 3 provides a comparison between the uncorrected B_{ATN} from the CLAP at all three
462   wavelengths, as well as photoacoustic B_{abs} interpolated to those wavelengths using AAE. For each
463   wavelength, the slopes are significantly greater than one. Moreover, there is an apparent
464   dependency on SSA and AAE in the agreement between the instruments. This is most obvious in
465   Fig. 3a (652 nm), where data with lower SSA and lower AAE (smaller markers, "brighter" colors)
466   fall below the best-fit line, while data with higher SSA and higher AAE (larger markers, "darker"
467   colors) fall above the best-fit line. This phenomenon is less clear in Fig. 3b-3c, but an apparent
468   dependency on SSA and AAE remains, which highlights the need to include both of these aerosol
469   optical properties (and appropriate interaction terms) when correcting B_{ATN} values.
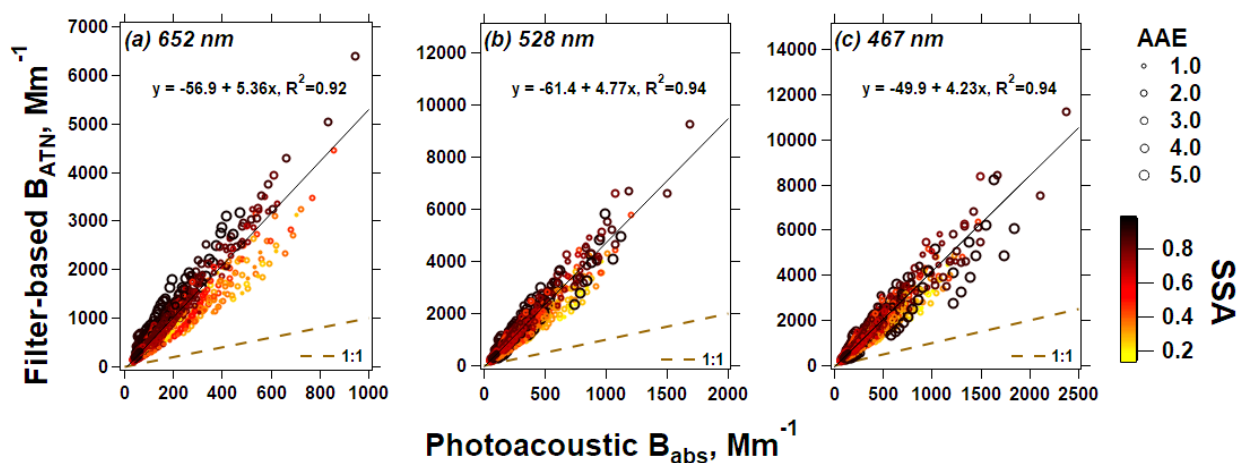
470

471   **Figure 3.** Comparison of the uncorrected CLAP-derived B_{ATN} and the reference B_{abs} at 652, 528,
472   and 467 nm for the FIREX data. The data points are colored by the corresponding SSA at the given
473   wavelength. The size of data points reflects their AAE quantified by the two PAX. The solid line
474   represents the linear regression, while the dashed line is a 1:1 line.

475   We first apply "Algorithm A" to the CLAP B_{ATN} data in Fig. 3. Using the reference B_{abs} values
476   from the PAX (in addition to B_{scat} values), we are able to derive a set of coefficients that enable
477   the correction of the data (Table 4). Corrected CLAP values are presented in Fig. 4 with the linear

478 relationships presented in Table 5. The slope for each wavelength is very close to the 1:1 line,
479 suggesting that our approach works well in correcting these data. Moreover, the heteroscedasticity
480 that exists in Fig. 3 has been minimized after correction, and there are no apparent trends in how
481 the data are organized in Fig. 4 due to the aerosol optical properties.

482 **Table 4** Coefficient values for Eq. (9) derived using "Algorithm A". We recommend these as the
483 initial guesses when implementing "Algorithm B" [a].

		G_0	G_1	G_2	G_3	G_4	G_5	G_6	G_7
CLAP (FIREX)	652 nm	0.27	-0.16	-0.18	-0.05	0.18	0.08	-0.01	0.03
	528 nm	0.30	-0.28	-0.18	-0.07	0.25	0.10	0.13	-0.17
	467 nm	0.32	-0.38	-0.20	-0.08	0.33	0.12	0.24	-0.31
TAP (FIREX)	652 nm	0.45	-0.45	0.07	-0.19	0.94	0.10	0.26	-0.35
	528 nm	0.54	-0.51	0.02	-0.26	0.76	0.20	0.38	-0.44
	467 nm	0.62	-0.59	-0.07	-0.32	0.73	0.29	0.53	-0.60
CLAP (SGP)	652 nm	0.37	-0.18	-0.34	-0.11	0.30	0.18	-0.36	0.41
	528 nm	0.40	-0.15	-0.42	-0.14	0.10	0.24	-0.17	0.25
	467 nm	0.43	-0.16	-0.45	-0.16	0.07	0.27	-0.06	0.12
PSAP (SGP)	652 nm	0.24	0.35	-0.16	-0.04	-0.47	0.07	-0.57	0.73
	528 nm	0.30	0.48	-0.26	-0.10	-0.67	0.17	-0.63	0.77
	467 nm	0.35	0.49	-0.34	-0.15	-0.69	0.23	-0.55	0.79
AETH (FIREX)	950 nm	0.47	0.17	0.01	-0.27	-0.4	0.25	-0.12	0.27
	880 nm	0.34	0.13	0.13	-0.17	0	0.10	-0.13	0.12
	660 nm	0.28	0.09	0.11	-0.12	0.15	0.05	-0.12	0.03
	590 nm	0.16	-0.08	0.26	-0.03	0.59	-0.08	-0.02	-0.19
	520 nm	0.16	-0.05	0.14	-0.01	0.54	-0.07	-0.02	-0.21
	470 nm	0.14	-0.05	0.06	0	0.53	-0.05	-0.02	-0.17
	370 nm	0.13	-0.09	0.11	0	0.59	-0.06	-0.01	0.01

484 [a] The coefficients derived from FIREX may be more appropriate for biomass burning aerosols, and
485 the coefficients derived from SGP may be more appropriate for rural background environments in
486 the absence of marine aerosols and dust (see Fig. S15).
487
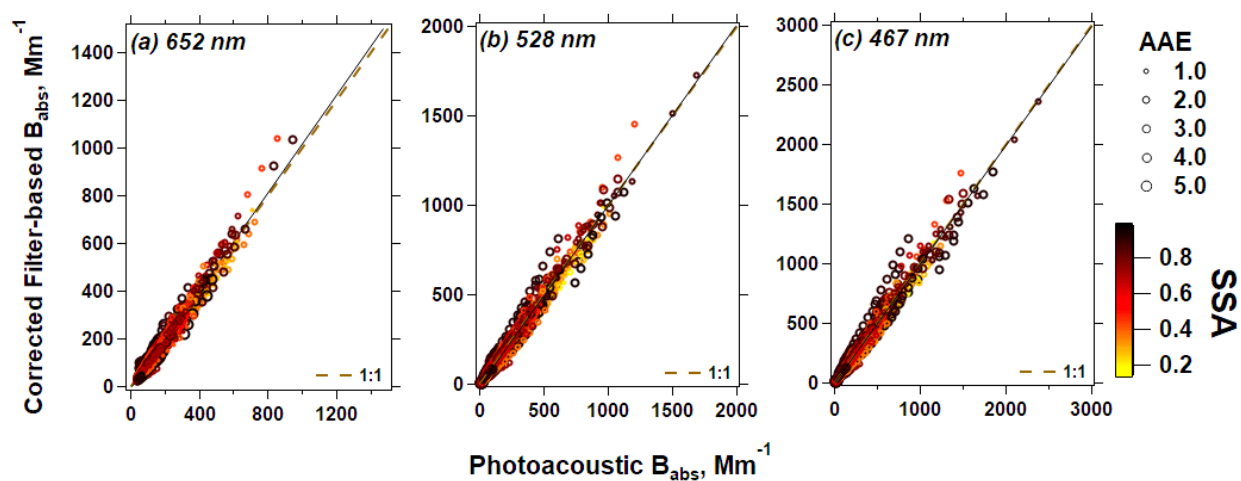
488
489 **Figure 4.** As in Fig. 3, but the CLAP-based B_{ATN} values have been corrected using our "Algorithm
490 A".

Table 5 Relationship between the filter-based B_{abs} corrected by "Algorithm A" and the reference B_{abs} at the operating wavelengths for the filter-based instrument. The relationship is achieved using major axis regression (Ayers, 2001). The value in the parentheses represents the coefficient of determination (R^2) for the linear relationship.

		652 nm	528 nm	467 nm
FIREX	**CLAP**	y = -7.8 + 1.02x (0.98)	y = -6.2 + 1.01x (0.98)	y = -3.2 + 1.00x (0.98)
	TAP	y = -10 + 1.00x (0.87)	y = -13 + 0.99x (0.87)	y = -16 + 0.99x (0.88)
SGP	**CLAP**	y = -0.25 + 1.08x (0.68)	y = -0.21 + 1.05x (0.67)	y = -0.04 + 0.99x (0.68)
	PSAP	y = -0.28 + 1.10x (0.43)	y = -0.24 + 1.06x (0.55)	y = -0.07 + 1.00x (0.62)

		950 nm	880 nm	660 nm	590 nm
FIREX	**AETH**	y = -3.19 + 1.01x (0.82)	y = -3.92 + 1.02x (0.85)	y = -5.97 + 1.03x (0.88)	y = -5.63 + 1.02x (0.90)
		520 nm	470 nm	370 nm	-
		y = -2.36 + 0.99x (0.90)	y = 2.93 + 0.95x (0.88)	y = 18.38 + 0.89x (0.80)	-

We next investigate the repeatability of the coefficient values presented in Table 4 by randomly selecting half of the measurements (N = 1338) from the whole FIREX dataset. By implementing "Algorithm A" to the extracted observations, we obtain new coefficient values for G_0 to G_7. This is repeated 1000 times to obtain a distribution of coefficient values (Fig. S13). The extraction approach mimics the process of obtaining new biomass burning datasets, so that we can estimate the variability of these derived coefficients. From Fig. S13 and Table S12, the derived coefficients are mostly insensitive to the different randomly-extracted datasets; most of the quartile deviation (defined as (Q3-Q1)/2, where Q1 and Q3 are the first and third quartile respectively) is within 0.05, except G_4 which has a quartile deviation of ~0.08. Consequently, the coefficient values obtained in "Algorithm A" appear to be reasonable initial guesses to correct filter-based absorption measurements during biomass burning events when the reference B_{abs} is unavailable, such as in "Algorithm B" and "Algorithm C".

We next implement "Algorithm B" to the CLAP B_{ATN} data from Fig. 3 using the initial guesses of the coefficients derived from "Algorithm A" (Table 4) along with reference B_{scat} values. To get a sense of the variability in the results, we randomly select half of the data and applied the correction; this process is repeated 1000 times. For each iteration, we compare the corrected B_{abs} from the CLAP to the reference B_{abs} from the PAX; the resulting slope, intercept, and R^2 values are summarized as box-and-whisker plots in Fig. 5. For all three wavelengths, the slopes are close to unity, and there is good correlation between the two absorption measurements ($R^2 \approx 0.98$), which indicates that the good performance seen in Fig. 4 is independent of the reference B_{abs} measurements and our algorithm is able to correct "new" B_{ATN}. Consequently, when scattering measurements are co-located with filter-based absorption measurements, our new correction algorithm performs well.

519
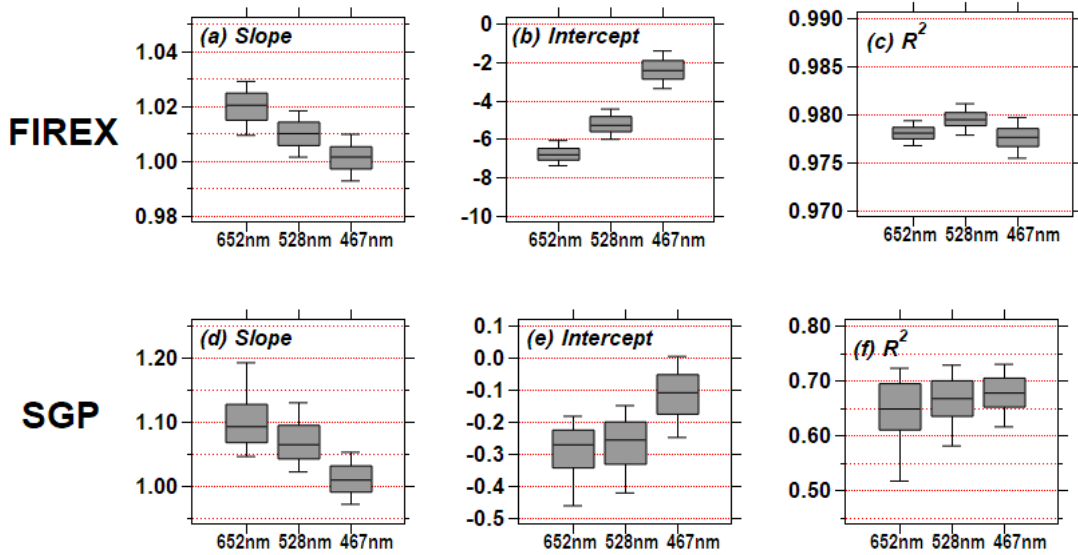
Figure 5. The box-and-whisker plots for the slope, intercept, and R^2 of the relationship between the CLAP-derived B_{abs} (corrected by "Algorithm B" in the present work) and PAX-derived B_{abs} for all three wavelengths. For details on how these values were generated, please refer to the text.

Lastly, we apply "Algorithm C" to the data in Fig. 3. However, we first require a functional relationship between AAE and SSA, because in this scenario, the CLAP B_{ATN} values are the only data input to the algorithm (and therefore, SSA is unknown). Liu et al. (2014) proposed that a power function can describe this relationship ($AAE = a + b \times SSA^c$); we present these data from FIREX along with power function fits (and associated prediction intervals) in Fig. 6. To define AAE in this figure, we fit a power-law relationship to the three B_{ATN} values from the CLAP; similarly, we define SSA using interpolated B_{scat} from the PAX and B_{ATN} from the CLAP (The rationale for using B_{ATN} is that if "Algorithm C" were to be implemented in practice, only B_{ATN} would be available). In Fig. 6, the data points are colored by "prediction error", effectively a metric to quantify how well the power function reproduces the individual data points. Although there is a fair amount of error in some of these points, we still obtain an SSA-AAE relationship required to initialize "Algorithm C".

535
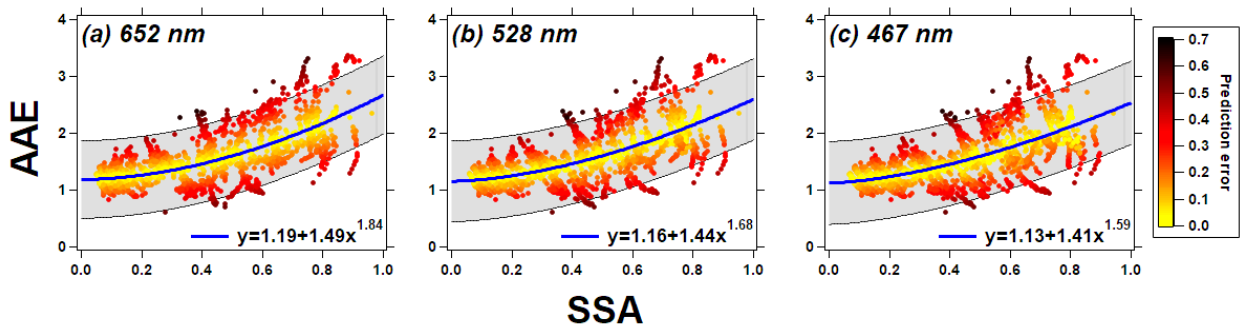
Figure 6. AAE plotted against SSA for the FIREX data. In the figures, AAE was computed using a power-law fit across all three wavelengths, and SSA was computed using the interpolated B_{scat}

538 from the two PAX and the reported B_{ATN} from the CLAP. The data points are colored by their
539 prediction error ((“true” AAE - “calculated” AAE)/ “calculated” AAE).

540 Even though there is uncertainty in the SSA vs. AAE relationship used in “Algorithm C”, after
541 corrections have been applied, the filter-based B_{abs} for the CLAP agrees well with the independent
542 reference B_{abs}; the slopes for all wavelengths are slightly greater than 1 (1.03-1.05) and the R^2
543 values are all high (0.97-0.98). However, even though the absorption measurements are corrected
544 well, there still remains large uncertainties in values of inferred scattering. Examples of this are
545 provided in Fig. 7, where we compare the SSA inferred from the PAX to the SSA inferred from
546 “Algorithm C” as well as B_{scat} for each wavelength. Generally speaking, data that are better
547 represented by the SSA vs. AAE relationship (i.e., smaller prediction error) results in better
548 agreement with the reference for both SSA and B_{scat}, but there is also a clear divergence from the
549 1:1 line in Fig. 7a-c as SSA decreases. Therefore, even though “Algorithm C” performs well at
550 correcting filter-based B_{ATN} to agree with the reference B_{abs}, estimates of final SSA values should
551 be considered to be uncertain.
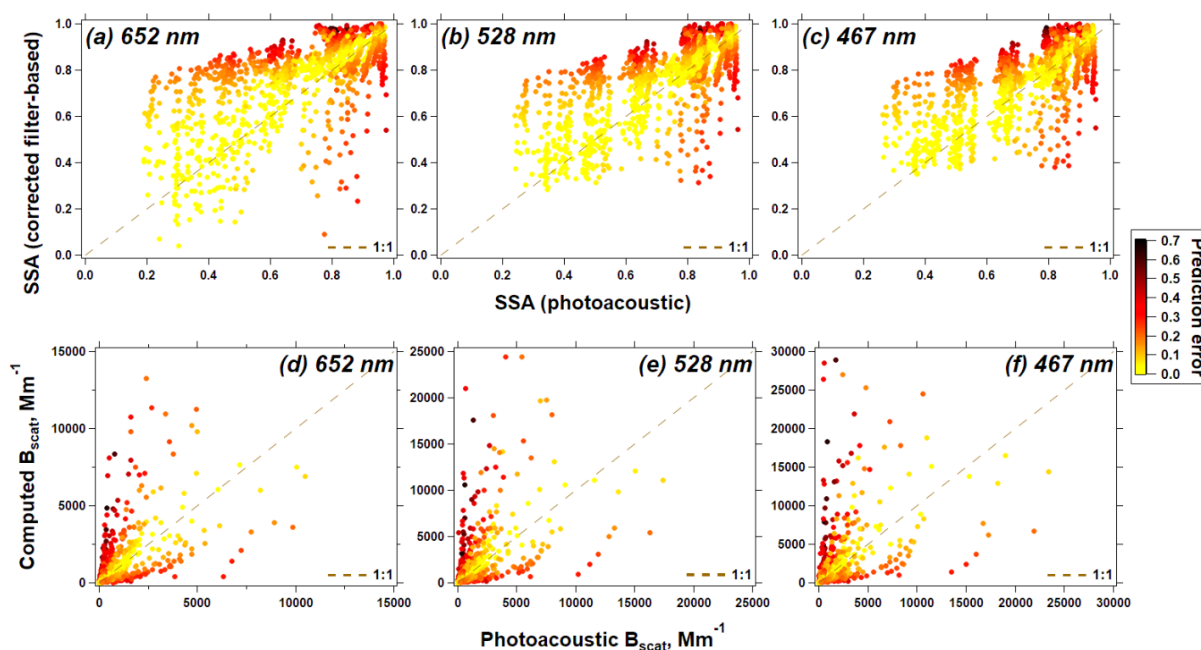
552

553 **Figure 7.** Comparison of SSA (a-c) and B_{scat} (d-f) at the three wavelengths for the FIREX data.
554 Vertical axis: values output from “Algorithm C”; horizontal axis: values calculated using the
555 photoacoustic B_{abs} and B_{scat}.

556 To explore the generalization of the new algorithms across different instruments, we next apply
557 our algorithms to the other filter-based absorption photometers operated during the FIREX study
558 (TAP and AETH). Consistent with what we observed for the CLAP results, the corrected TAP-
559 and AETH-derived B_{abs} is in good agreement with the photoacoustic B_{abs} (as demonstrated in Table
560 4 and Table 5, as well as Fig. S11-S12). Moreover, the corrected B_{abs} from the three filter-based
561 instruments agrees with each other for all three wavelengths (Table 6), confirming the consistency
562 of our algorithm.

Table 6 Inter-comparison between different filter-based B_{abs} corrected by "Algorithm A" in the present work. The value in the parentheses represents the coefficient of determination (R^2) of the linear relationship.

	FIREX: CLAP vs. TAP	FIREX: CLAP vs. AETH	FIREX: TAP vs. AETH	SGP: CLAP vs. PSAP
652 nm	y = 1.84 + 1.02x (0.89)	y = 4.17 + 0.94x (0.87)	y = -0.31 + 0.99x (0.82)	y = -0.04 + 0.99x (0.70)
528 nm	y = 5.75 + 1.02x (0.88)	y = 3.70 + 0.91x (0.85)	y = -6.38 + 0.98x (0.82)	y = -0.11 + 1.02x (0.73)
467 nm	y = 10.57 + 1.01x (0.88)	y = 0.45 + 0.98x (0.83)	y = -13.62 + 1.04x (0.79)	y = -0.11 + 1.02x (0.76)

3.3. Application of the new algorithms to ambient data

To test our algorithms further, we extended our work to ambient data collected the DOE SGP site during the time period which the PASS-3 was operational. From the SGP data, we derived a different set of coefficients for ambient data using "Algorithm A", which differ from those derived for FIREX (Table 4). The results presented in Fig. 8 and Table 5 suggest that our new algorithm works at least as well as B1999 and V2005 on this dataset (both with updated coefficients). The repeatability of the coefficient values in "Algorithm A" is confirmed for the SGP measurements using the same procedure as described in Sect. 3.2 (see results in Fig. S13 and Table S12).
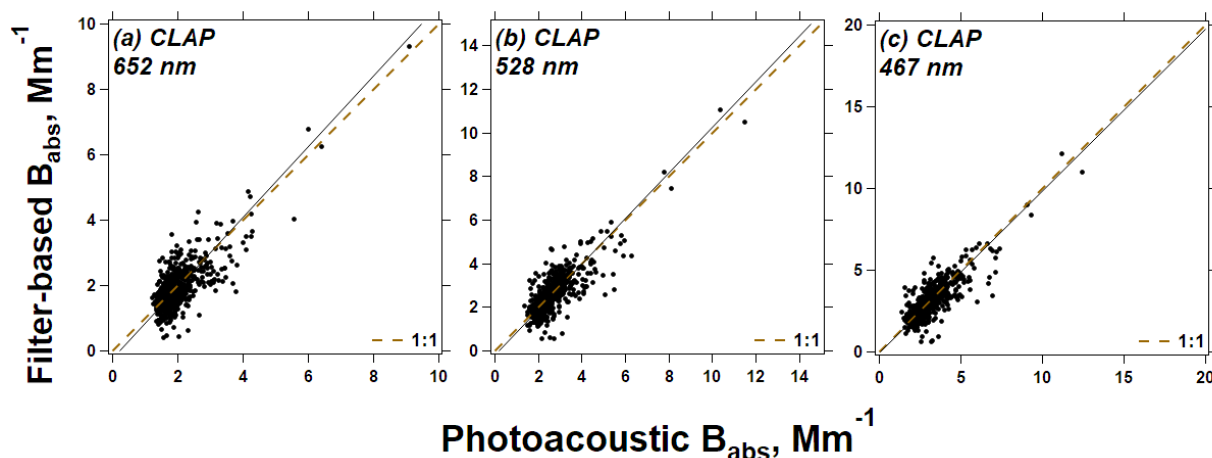
Figure 8. Inter-comparison between the CLAP-derived B_{abs} corrected by "Algorithm A" in the present work and reference B_{abs} at 652, 528, and 467 nm for the ambient data at the SGP study area. The solid line represents the linear regression, while the dashed line is a 1:1 line.

On the SGP data, we see similar performance to the FIREX data when we apply "Algorithm B", where we again sampled half of the CLAP data, used the initial guesses derived in "Algorithm A", and repeated this process 1000 times. Although the slopes tend to be larger than 1 (i.e., the corrected CLAP B_{abs} remains high relative to the PASS B_{abs}), the results still represent an improvement over B1999 and V2005 using their recommended coefficients for their correction equations.

Implementing "Algorithm C" is challenging for ambient data, because there is no distinct power function relationship in AAE vs. SSA (Fig. 9); this is consistent with other field studies reporting both SSA and AAE (e.g., Backman et al. (2014) and Lim et al. (2018)). Our approach described

588 here is only appropriate for ambient aerosols that follow a power function, such as sites impacted
589 by biomass burning. Nevertheless, we did apply this to a subset of the SGP data where the AAE-
590 SSA prediction error is within 30% (N = 86), and for this subset of data, "Algorithm C" works
591 fairly well (slopes ≈ 0.95; see Fig. S14). Therefore, while "Algorithm C" may have utility for
592 ambient data, we advise caution when using this algorithm since the aerosols influencing the site
593 may not be represented by a clear AAE-SSA power function (e.g., when biomass burning and
594 coarse aerosols are equally prevalent at a long-term monitoring site).
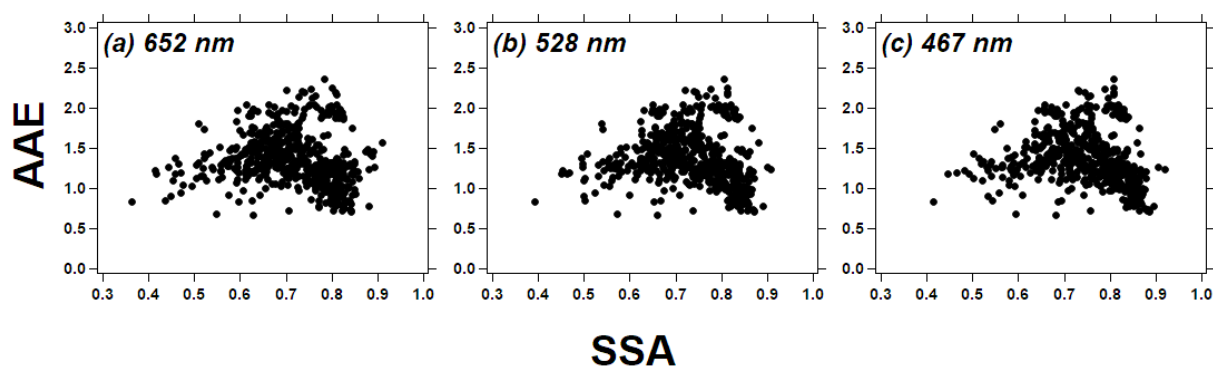
595

596 **Figure 9.** AAE plotted against SSA for the SGP ambient data. The power law fit (AAE = a + b × SSA^c)
597 is performed on SSA (SSA = $B_{scat}/(B_{scat} + B_{ATN})$) and AAE computed by three-wavelength B_{ATN}.

598 These new algorithms are also applicable to the PSAP deployed at the SGP site. The results of the
599 correction for the PSAP are presented in Table 5 and Fig. S11, and the recommended initial guesses
600 when implementing "Algorithm B" to PSAP-B_{ATN} at ambient environments are given in Table 4.
601 As expected, there is good agreement between corrected PSAP- and CLAP-B_{abs} (Table 6).

602 To investigate if our algorithms are suitable to correct B_{abs} obtained from different ambient
603 environments, the aerosol properties from the SGP site are compared to those from the other
604 NOAA/ESRL observational sites. We use the similar "AAE-SAE space" as that in Cappa et al.
605 (2016) and Schmeisser et al. (2017) to infer dominant aerosol types (e.g., BC, BrC, dust, mixed
606 dust/BC/BrC, see Fig. S15). Our results of AAE and SAE overlap with most of the values from
607 the NOAA/ESRL sites, except when marine aerosols or dust contribute to the local aerosol
608 emissions. Though none of the NOAA/ESRL sites fall into the clusters of BC or BC/BrC, some of
609 our data can represent the optical properties of aerosols from these clusters. Therefore, we highlight
610 that our algorithm developed by the SGP data may have the potential to be generalized to a variety
611 of environmental conditions, but we would need to validate this using observations from more
612 studies.

613 3.4. Impact of the implemented correction algorithm on aerosol optical properties

614 In addition to the direct comparisons of B_{abs} between the filter-based and photoacoustic
615 measurements, we compare derived optical properties (AAE and SSA) from different instruments
616 to assess the algorithms' performance on derived aerosol optical properties. For example, we have
617 discussed the discrepancy of SSA between the filter-based and photoacoustic measurements when
618 implementing "Algorithm C" in Sect. 3.2. In this section we will more broadly discuss the impact
619 of different correction algorithms on AAE and SSA.

620 In Fig. 10, we present the frequency distribution of AAE for both FIREX and SGP data generated
621 from different campaign/instrument pairs using different correction approaches. For the FIREX
622 data (Fig. 10a-b), most corrections (with the exception of the "default" B1999) are consistent with
623 the photoacoustic data, while for the SGP data (Fig. 10c-d), most corrections (with the exception
624 of "default" V2005) are consistent with the photoacoustic data. However, updating the coefficients
625 for B1999 and V2005 improves the agreement with the photoacoustic data. The 50% difference
626 that exists between the B1999 and V2005 algorithms in all panels in Fig. 10 are consistent with
627 previous studies. For example, both Backman et al. (2014) and Davies et al. (2019) found that the
628 V2005-derived AAE is greater than B1999-derived AAE by 33% to 50% for ambient aerosols.
629 Therefore, we highlight that the default coefficients in B1999 and V2005 may have some
630 limitations when deriving AAE using the corrected B_{abs}; instead, updating the coefficients or using
631 the new algorithm proposed in this work may yield more robust AAE results.

632
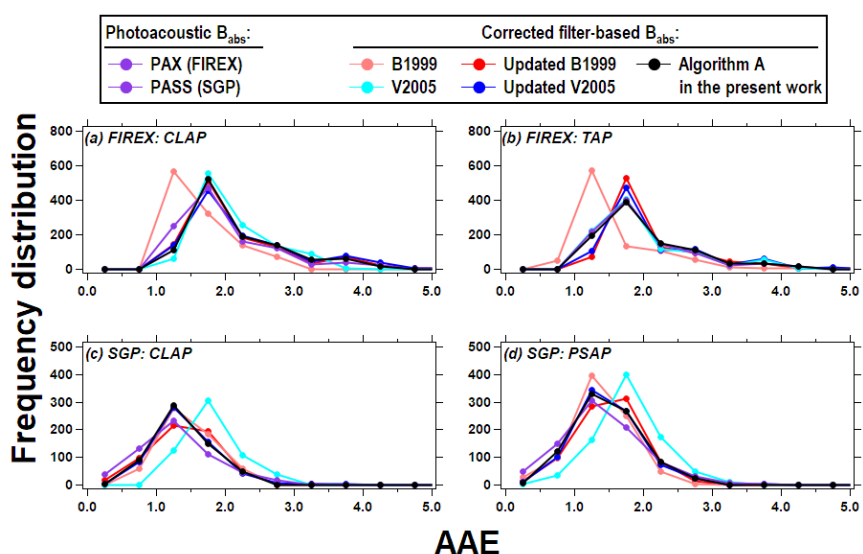
Figure 10. The frequency distribution of AAE calculated for different instrument/correction
combinations of multi-wavelength B_{abs}.

635 Similar to Fig. 10, we also investigate the distribution of SSA computed by using corrected B_{abs}
636 along with B_{scat}. We provide the results at 652 nm as an example in the main text (Fig. 11); figures
637 for 528 nm and 467 nm can be found in the Supplementary Material (Fig. S16 and S17). For both
638 FIREX and SGP data, the SSA obtained using the new algorithm agree very well with the B1999
639 and V2005 but only when their coefficients have been updated. Calculations of SSA using B1999
640 and V2005 with their recommended coefficients suggest that these values may be biased low,
641 which follows the over-estimation of corrected B_{abs} demonstrated in Fig. 2.

642
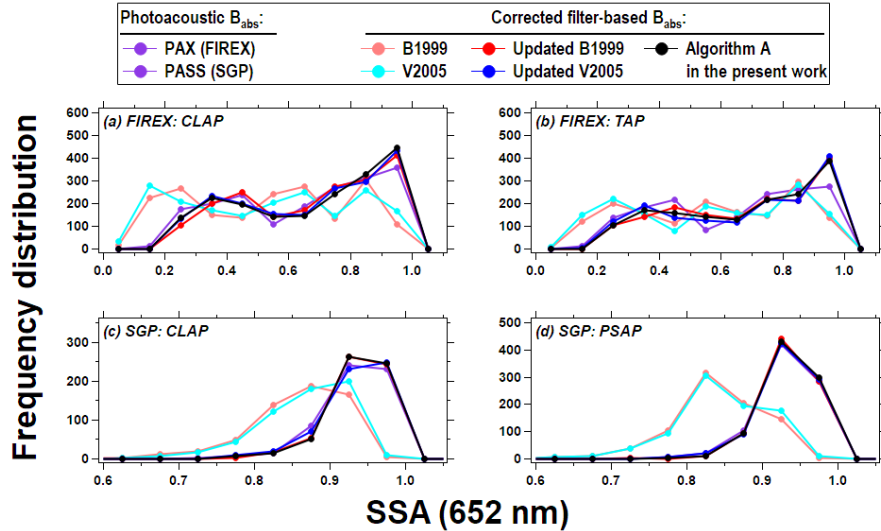
Figure 11. The frequency distribution of SSA (652 nm) calculated for different instrument/correction combinations of B_{abs} and B_{scat}.

Moreover, we plot similar figures as Fig. 10-11 using all algorithms (A, B, and C). As shown in Fig. S18, the results using "Algorithm B" agrees very well with those using "Algorithm A", but the use of "Algorithm C" results in some obvious discrepancies compared to the photoacoustic reference, again highlighting the potential for large uncertainty using this algorithm.

In Fig. 12, we directly compare the distributions of both AAE and SSA at 652 nm for all of the filter-based absorption photometers considered here, using our "Algorithm A" to correct the B_{ATN} data. For both datasets, after the corrections have been applied, there are only marginal differences of the AAE (Fig. 10a and 10b) derived by different instruments. Similarly, there is good agreement among the SSA values when using corrected-B_{abs} from different instruments (Fig. 10c and 10d). Overall, the derived properties using the new correction are consistent across all instruments, suggesting its generalizability.

656
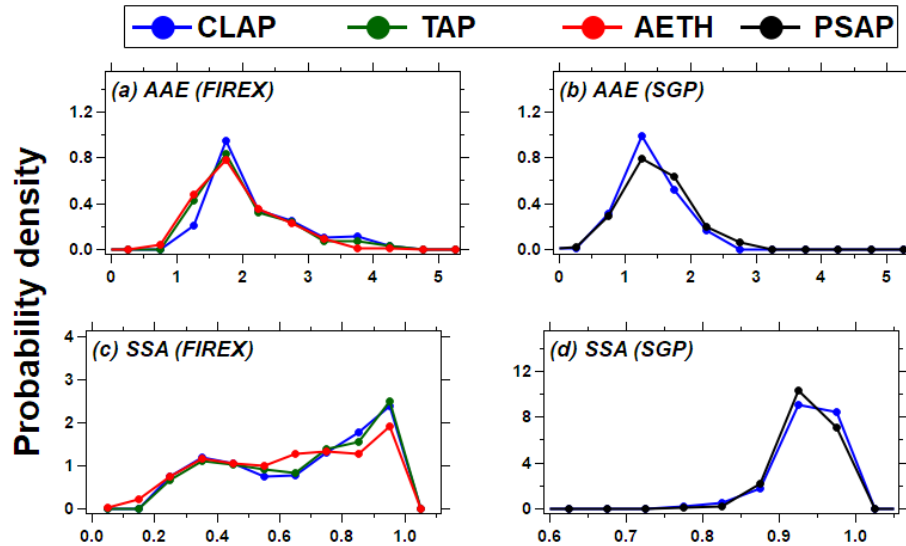
Figure 12 The probability density of AAE and SSA (652 nm) derived by different filter-based photometers B$_{abs}$ (corrected by "Algorithm A" in the present work). Note that the number of total observations vary across instruments.

660   3.5. Uncertainty of the new algorithms

661   In this section, we estimate the uncertainty of the new algorithms due to both measurement
662   uncertainties of the instruments and the uncertainties of parameter computation. We then simulate
663   the propagated uncertainty in the corrected filter-based B$_{abs}$ reported in this paper.

664   Measurement uncertainties of the instruments considered here have been reported in previous work
665   (e.g., (Anderson et al., 1996; Nakayama et al., 2015; Ogren et al., 2017; Sherman et al., 2015)) and
666   are summarized in Table 1. The typical sources of measurement uncertainty of the aerosol
667   instruments include: 1) instrument noise (often associated with the averaging time); 2) calibration
668   uncertainties (such as the accuracy of the operating wavelengths and the properties of the
669   calibration materials); 3) standard temperature and pressure (STP) correction uncertainties
670   (Sherman et al., 2015); and 4) flow rate uncertainties. Additional uncertainties that are specific to
671   filter-based absorption photometers include spot size and filter medium corrections (Bond et al.,
672   1999; Ogren et al., 2017). Regardless, these values all tend to be ≤ 30%, which is consistent with
673   other commonly-used aerosol instrumentation.

674   Because correction algorithms for filter-based absorption instruments also require aerosol optical
675   properties, the algorithms' performance will be affected by these values as well. For example,
676   uncertainties in SSA are directly related to uncertainties associated with B$_{abs}$ and B$_{scat}$, which are
677   both included in our simulations. However, capturing uncertainties in AAE is more complex, as
678   AAE can be computed by either "2λ fit" (a linear fit using B$_{abs}$ at two wavelengths) or "3λ fit"
679   (same as the power fit used in the present work). Davies et al. (2019) used the 3λ fit to calculate
680   AAE and compared this to calculations using 662 nm and 785 nm (i.e., AAE$_{662/785}$), finding that
681   the 3λ results was about 50% greater. Moreover, similar differences (-35% to 85%) can exist
682   comparing two different 2λ combinations (AAE$_{440/870}$ and AAE$_{675/870}$), depending on the
683   contribution of brown carbon to absorption at 440 nm (Wang et al., 2016). However, based on Fig.
684   S19 and S20, we demonstrate small (< ~10%) differences in the calculated values of AAE using

685   our Algorithm A using different 2λ combinations for linear fits and the 3λ power-law fit, when
686   considering both FIREX and SGP data. Consequently, we do not include AAE calculation
687   uncertainty in our simulation.

688   In our simulations, the propagated uncertainty of corrected B_{abs} is estimated by implementing the
689   new algorithm to datasets in which filter-based B_{ATN}, reference B_{abs}, and B_{scat} are subject to
690   measurement uncertainties. The full procedure is outlined in the Supplementary Material, but we
691   provide a brief overview of our Monte Carlo approach here. First, we create a synthetic dataset (n
692   = 500 records) that defines B_{abs} at 652 nm and AAE that is intended to represent biomass burning.
693   Values of B_{ATN} and SSA are then computed using the relationships presented in Fig. 3 and Fig. 6,
694   respectively. Respective uncertainties associated with each of these values are applied following
695   Table 1, assuming that these follow a normal distribution. We then applied "Algorithm B" to the
696   B_{ATN} dataset, repeated 1000 times, to quantify overall uncertainty associated with our correction
697   algorithm.

698   Figure 13 provides a graphical summary of our uncertainty simulation results, which was derived
699   by fitting linear equations to the "true" B_{abs} value (that we defined) and the "corrected" B_{abs} values
700   (outputs of each iteration). Considering the slopes (Fig. 12a), our algorithm can generally
701   reproduce the "true" value within 10% at 652 nm and 528 nm, but the performance is slightly
702   degraded at 467 nm. The median intercept for our simulations is close to zero, but the interquartile
703   range increases with decreasing wavelength (Fig. 12b), suggesting that the uncertainty may
704   increase at shorter wavelengths. The coefficients of determination (Fig. 12c) range from 0.47 (652
705   nm) to 0.68 (467 nm), showing that the algorithm may be less precise if large measurement
706   uncertainties exist. Even though these sources of uncertainty exist when implementing our
707   correction algorithms and propagate through to the corrected values, we argue that our new
708   algorithm will "standardize" uncertainties across corrected B_{abs} values from filter-based absorption
709   photometers. Moreover, the new algorithms perform, at least, better than the previous algorithms
710   with "default" coefficients, or as well as the previous algorithms with updated coefficients.
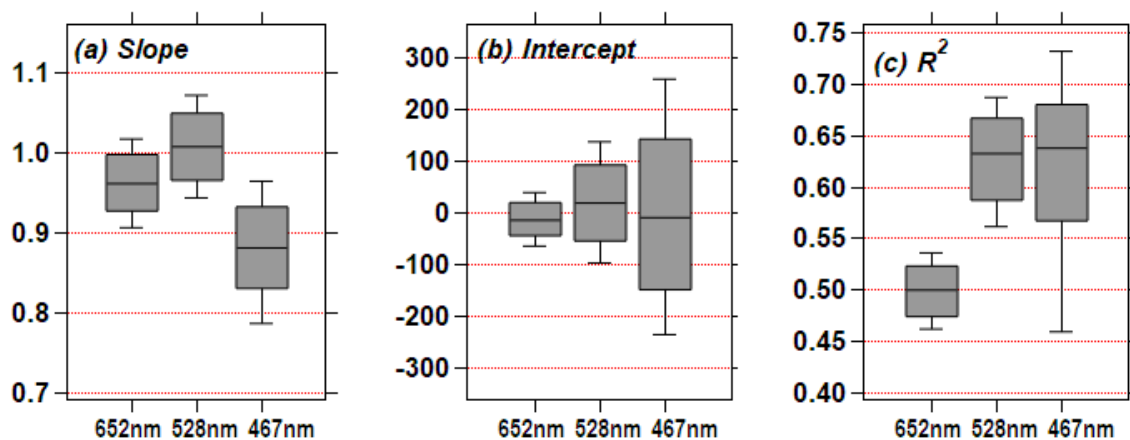
711

712   **Figure 13.** The box-and-whisker plots (slope, intercept, and R^2) for the Monte Carlo simulation of
713   the relationship between the CLAP-derived B_{abs} (corrected by "Algorithm B" in the present work)
714   and "true" B_{abs} for all three wavelengths.

4. Conclusions

Filter-based absorption instruments are widely used at global observational sites due to their relatively low cost, fast response, and easy operation. Despite the existence of different correction algorithms to correct the filter-based B_{abs} measurements, these are not "standardized" as differences in corrected B_{abs} values exist across different instrument/correction combinations, even when the instruments are co-located. This study provides a systematic evaluation of the previous correction algorithms (B1999 and V2005 corrections) on the CLAP and similar instruments (TAP and PSAP) using both laboratory-generated biomass burning emissions and ambient aerosols. We also developed new correction algorithms that are applicable to any filter-based absorption photometer (e.g., PSAP, CLAP, TAP, AETH), which will have utility for any historic or future filter-based absorption measurements and which have the potential to standardize absorption coefficients across all filter-based instruments. This latter point is demonstrated in Table 6 and Fig. 12 in that there is good agreement across all filter-based absorption photometers when applying our corrections to both biomass burning and ambient data. In practice, we anticipate that our Algorithm B will be most common, because at long-term monitoring sites, filter-based absorption photometers are typically co-located with a nephelometer.

Using the existing corrections on our CLAP measurements, we find that the corrected B_{abs} overestimate photoacoustic B_{abs} by factors of ~2.6 (biomass burning aerosols) and ~3.2 (ambient aerosols). Similar overestimations of absorption by filter-based instruments are seen in the results of TAP from the FIREX study and PSAP deployed at the SGP. Comparing between B1999 and V2005, B_{abs} corrected by the two corrections differ by -6% to 18%. These discrepancies in our results are consistent with those reported for the inter-comparisons between filter-based and photoacoustic absorption instruments (e.g., (Arnott et al., 2003; Davies et al., 2019; Li et al., 2019; Müller et al., 2011a)).

Overall, our new developed algorithms (A, B, and C) perform well on correcting B_{abs} for different filter-based absorption photometers (CLAP, TAP, PSAP, and AETH) from both biomass burning and ambient measurements. Our work suggests that if the filter-based instrument is co-operated with a reference absorption instrument and a NEPH at field for a period, researchers can compute site-specific initial guesses (same as "Algorithm A" in the present work). Otherwise, either "Algorithm B" or "Algorithm C" proposed in this paper can be used to correct the filter-based measurements. In "Algorithm B" when a filter-based absorption photometer is co-located with a NEPH but without a reference instrument, the set of coefficients yield in this work (Table 4) can be used as initial guesses to implement the algorithm. In "Algorithm C" when a filter-based absorption photometer is operated by itself, a "representative" relationship between AAE and SSA can be used to estimate SSA from AAE at each step in the iterative process, but we advise caution if this relationship is not monotonic (e.g., as in the ambient data from SGP and from Backman et al. (2014) and Lim et al. (2018)). The only scenario not included in the present work is that the filter-based absorption photometer is co-located with a reference absorption instrument, but no instrument for scattering. However, under this scenario, one could simply use the photoacoustic B_{abs} data because no filter-induced biases exist for those instruments.

In terms of the aerosol optical properties (AAE and SSA) computed by different corrections, the new algorithm suggests no bias of AAE and SSA when compared to that derived by updated-B1999and updated-V2005 for both aerosol datasets.

However, the new algorithm is not without limitations. First, we used the photoacoustic B_{abs} as the reference to develop the algorithm and the initial guess of the coefficients; meanwhile, some studies argue that photoacoustic absorption is not a "ground truth" (e.g., (Lack et al., 2006; Lewis et al., 2008)). Thus, we simulate the propagated uncertainty of our algorithms considering the measurement uncertainties due to the photoacoustic B_{abs} (as well as B_{ATN} and B_{scat}) and find that the corrected B_{abs} can be biased by -17% to 5%, depending on the operated wavelength. Although potential bias due to the precision of photoacoustic B_{abs} cannot be excluded, using our new algorithm to correct the filter-based B_{abs} will at least eliminate correction-related biases among different filter-based instruments. Second, we only tested the algorithms with data from biomass burning and ambient measurements. It is unclear how the algorithms will work for other absorbing aerosols (e.g., dominated by fossil fuel emissions or mineral dust). Further evaluation of the performance of the new algorithm on other aerosol sources may help to address this issue. Regardless, we argue that our approach can standardize reported absorption coefficients at long-term monitoring sites, which has the potential to yield a better data set with which to evaluate chemistry-climate models.

Code and data availability. The code for the algorithm was initially written in Igor Pro (WaveMetrics Inc.) and has been developed to be accessible through either Python (Version 3.7.5) or Igor Pro. The implementation of our algorithm is available at https://doi.org/10.5281/zenodo.3742342. The FIREX aerosol products are available at https://esrl.noaa.gov/csd/project/firex. The SGP aerosol products are available at https://www.archive.arm.gov/discovery/ (February 2013–July 2013, 36° 36′ 18.0″ N, 97° 29′ 6.0″ W: Southern Great Plains Central Facility, data set accessed 01/16/19).

Author contributions. HL developed the model, conducted the evaluations, and drafted the manuscript. AAM and GRM edited the manuscript and obtained funding.

Competing interests. The authors declare that they have no conflict of interest.

Acknowledgements. The authors would like to thank Allison Aiken (Los Alamos National Laboratory) for useful discussions regarding the SGP PASS-3 data. The authors greatly acknowledge Vanessa Selimovic, and Robert Yokelson from University of Montana for lending us the PAX-405; Patrick Sheridan, John Ogren, and Derek Hageman from NOAA for lending us the CLAP; and Anthony Prenni from the National Park Service for lending us the AETH during the FIREX campaign. We also thank Nick Good (Colorado State University), Jim Roberts (NOAA) and Carsten Warneke (NOAA) for their on-site support at FSL.

Financial support. The authors and FIREX data were supported by NOAA Climate Program Office Grant NA16OAR4310109. The ambient data at SGP site in Lamont (OK, USA) were obtained from the atmospheric radiation measurement (ARM) user facility, a U.S. Department of Energy (DOE) Office of Science user facility managed by the Office of Biological and Environmental Research.

Review statement. The authors thank Associate Editor Paolo Laj for handling this submission and the anonymous reviewers for their valuable comments.

797   5.   References

798   Allan, D. W.: Statistics of atomic frequency standards, Proc. IEEE, 54(2), 221–230,
799   doi:10.1109/PROC.1966.4634, 1966.

800   Alvarado, M. J., Lonsdale, C. R., Macintyre, H. L., Bian, H., Chin, M., Ridley, D. A., Heald, C.
801   L., Thornhill, K. L., Anderson, B. E., Cubison, M. J., Jimenez, J. L., Kondo, Y., Sahu, L. K., Dibb,
802   J. E. and Wang, C.: Evaluating model parameterizations of submicron aerosol scattering and
803   absorption with in situ data from ARCTAS 2008, Atmos. Chem. Phys., 16(14), 9435–9455,
804   doi:10.5194/acp-16-9435-2016, 2016.

805   Anderson, T. L., Covert, D. S., Marshall, S. F., Laucks, M. L., Charlson, R. J., Waggoner, A. P.,
806   Ogren, J. A., Caldow, R., Holm, R. L., Quant, F. R., Sem, G. J., Wiedensohler, A., Ahlquist, N. A.
807   and Bates, T. S.: Performance Characteristics of a High-Sensitivity, Three-Wavelength, Total
808   Scatter/Backscatter Nephelometer, J. Atmos. Ocean. Technol., 13(5), 967–986, doi:10.1175/1520-
809   0426, 1996.

810   Andrews, E., Sheridan, P. J. and Ogren, J. A.: Seasonal differences in the vertical profiles of
811   aerosol optical properties over rural Oklahoma, Atmos. Chem. Phys., 11(20), 10661–10676,
812   doi:10.5194/acp-11-10661-2011, 2011.

813   Andrews, E., Sheridan, P. J., Ogren, J. A., Hageman, D., Jefferson, A., Wendell, J., Alástuey, A.,
814   Alados-Arboledas, L., Bergin, M., Ealo, M., Hallar, A. G., Hoffer, A., Kalapov, I., Keywood, M.,
815   Kim, J., Kim, S.-W., Kolonjari, F., Labuschagne, C., Lin, N.-H., Macdonald, A., Mayol-Bracero,
816   O. L., McCubbin, I. B., Pandolfi, M., Reisen, F., Sharma, S., Sherman, J. P., Sorribas, M. and Sun,
817   J.: Overview of the NOAA/ESRL Federated Aerosol Network, Bull. Am. Meteorol. Soc., 100(1),
818   123–135, doi:10.1175/BAMS-D-17-0175.1, 2019.

819   Arnott, W. P., Moosmüller, H., Sheridan, P. J., Ogren, J. A., Raspet, R., Slaton, W. V., Hand, J.
820   L., Kreidenweis, S. M. and Collett, J. L.: Photoacoustic and filter-based ambient aerosol light
821   absorption measurements: Instrument comparisons and the role of relative humidity, J. Geophys.
822   Res., 108(D1), 4034, doi:10.1029/2002JD002165, 2003.

823   Arnott, W. P., Hamasha, K., Moosmüller, H., Sheridan, P. J. and Ogren, J. A.: Towards Aerosol
824   Light-Absorption Measurements with a 7-Wavelength Aethalometer: Evaluation with a
825   Photoacoustic Instrument and 3-Wavelength Nephelometer, Aerosol Sci. Technol., 39(1), 17–29,
826   doi:10.1080/027868290901972, 2005.

827   Ayers, G. P.: Comment on regression analysis of air quality data, Atmos. Environ., 35(13), 2423–
828   2425, doi:10.1016/S1352-2310(00)00527-6, 2001.

829   Backman, J., Virkkula, A., Vakkari, V., Beukes, J. P., Van Zyl, P. G., Josipovic, M., Piketh, S.,
830   Tiitta, P., Chiloane, K., Petäjä, T., Kulmala, M. and Laakso, L.: Differences in aerosol absorption
831   Ångström exponents between correction algorithms for a particle soot absorption photometer
832   measured on the South African Highveld, Atmos. Meas. Tech., 7(12), 4285–4298,
833   doi:10.5194/amt-7-4285-2014, 2014.

834   Bergstrom, R. W., Pilewskie, P., Russell, P. B., Redemann, J., Bond, T. C., Quinn, P. K. and Sierau,
835   B.: Spectral absorption properties of atmospheric aerosols, Atmos. Chem. Phys., 7(23), 5937–5943,
836   doi:10.5194/acp-7-5937-2007, 2007.

Bond, T. C. and Bergstrom, R. W.: Light absorption by carbonaceous particles: An investigative review, Aerosol Sci. Technol., 40(1), 27–67, doi:10.1080/02786820500421521, 2006.

Bond, T. C., Anderson, T. L. and Campbell, D.: Calibration and Intercomparison of Filter-Based Measurements of Visible Light Absorption by Aerosols, Aerosol Sci. Technol., 30(6), 582–600, doi:10.1080/027868299304435, 1999.

Boucher, O.: Atmospheric Aerosols, Springer Netherlands, Dordrecht., 2015.

Cappa, C. D., Lack, D. A., Burkholder, J. B. and Ravishankara, A. R.: Bias in Filter-Based Aerosol Light Absorption Measurements Due to Organic Aerosol Loading: Evidence from Laboratory Measurements, Aerosol Sci. Technol., 42(12), 1022–1032, doi:10.1080/02786820802389285, 2008.

Cappa, C. D., Kolesar, K. R., Zhang, X., Atkinson, D. B., Pekour, M. S., Zaveri, R. A., Zelenyuk, A. and Zhang, Q.: Understanding the optical properties of ambient sub- and supermicron particulate matter: results from the CARES 2010 field study in northern California, Atmos. Chem. Phys., 16(10), 6511–6535, doi:10.5194/acp-16-6511-2016, 2016.

Chen, S., Russell, L. M., Cappa, C. D., Zhang, X., Kleeman, M. J., Kumar, A., Liu, D. and Ramanathan, V.: Comparing black and brown carbon absorption from AERONET and surface measurements at wintertime Fresno, Atmos. Environ., 199, 164–176, doi:10.1016/j.atmosenv.2018.11.032, 2019.

Collaud Coen, M., Weingartner, E., Apituley, A., Ceburnis, D., Fierz-Schmidhauser, R., Flentje, H., Henzing, J. S., Jennings, S. G., Moerman, M., Petzold, A., Schmid, O. and Baltensperger, U.: Minimizing light absorption measurement artifacts of the Aethalometer: evaluation of five correction algorithms, Atmos. Meas. Tech., 3(2), 457–474, doi:10.5194/amt-3-457-2010, 2010.

Davies, N. W., Fox, C., Szpek, K., Cotterell, M. I., Taylor, J. W., Allan, J. D., Williams, P. I., Trembath, J., Haywood, J. M. and Langridge, J. M.: Evaluating biases in filter-based aerosol absorption measurements using photoacoustic spectroscopy, Atmos. Meas. Tech., 12(6), 3417–3434, doi:10.5194/amt-12-3417-2019, 2019.

Drinovec, L., Gregorič, A., Zotter, P., Wolf, R., Bruns, E. A., Prévôt, A. S. H., Petit, J.-E., Favez, O., Sciare, J., Arnold, I. J., Chakrabarty, R. K., Moosmüller, H., Filep, A. and Močnik, G.: The filter-loading effect by ambient aerosols in filter absorption photometers depends on the coating of the sampled particles, Atmos. Meas. Tech., 10(3), 1043–1059, doi:10.5194/amt-10-1043-2017, 2017.

Fischer, D. Al and Smith, G. D.: A portable, four-wavelength, single-cell photoacoustic spectrometer for ambient aerosol absorption, Aerosol Sci. Technol., 52(4), 393–406, doi:10.1080/02786826.2017.1413231, 2018.

Horvath, H.: Atmospheric light absorption—A review, Atmos. Environ. Part A. Gen. Top., 27(3), 293–317, doi:10.1016/0960-1686(93)90104-7, 1993.

Jiang, Y., Yang, J., Gagné, S., Chan, T. W., Thomson, K., Fofie, E., Cary, R. A., Rutherford, D., Comer, B., Swanson, J., Lin, Y., Van Rooy, P., Asa-Awuku, A., Jung, H., Barsanti, K., Karavalakis, G., Cocker, D., Durbin, T. D., Miller, J. W. and Johnson, K. C.: Sources of variance in BC mass measurements from a small marine engine: Influence of the instruments, fuels and loads, Atmos.

Environ., 182, 128–137, doi:10.1016/j.atmosenv.2018.03.008, 2018.

Kirchstetter, T. W. and Novakov, T.: Controlled generation of black carbon particles from a diffusion flame and applications in evaluating black carbon measurement methods, Atmos. Environ., 41(9), 1874–1888, doi:10.1016/j.atmosenv.2006.10.067, 2007.

Koss, A. R., Sekimoto, K., Gilman, J. B., Selimovic, V., Coggon, M. M., Zarzana, K. J., Yuan, B., Lerner, B. M., Brown, S. S., Jimenez, J. L., Krechmer, J., Roberts, J. M., Warneke, C., Yokelson, R. J. and de Gouw, J.: Non-methane organic gas emissions from biomass burning: identification, quantification, and emission factors from PTR-ToF during the FIREX 2016 laboratory experiment, Atmos. Chem. Phys., 18(5), 3299–3319, doi:10.5194/acp-18-3299-2018, 2018.

Lack, D. A., Lovejoy, E. R., Baynard, T., Pettersson, A. and Ravishankara, A. R.: Aerosol Absorption Measurement using Photoacoustic Spectroscopy: Sensitivity, Calibration, and Uncertainty Developments, Aerosol Sci. Technol., 40(9), 697–708, doi:10.1080/02786820600803917, 2006.

Lack, D. A., Cappa, C. D., Covert, D. S., Baynard, T., Massoli, P., Sierau, B., Bates, T. S., Quinn, P. K., Lovejoy, E. R. and Ravishankara, A. R.: Bias in Filter-Based Aerosol Light Absorption Measurements Due to Organic Aerosol Loading: Evidence from Ambient Measurements, Aerosol Sci. Technol., 42(12), 1033–1041, doi:10.1080/02786820802389277, 2008a.

Lack, D. A., Lerner, B., Granier, C., Baynard, T., Lovejoy, E., Massoli, P., Ravishankara, A. R. and Williams, E.: Light absorbing carbon emissions from commercial shipping, Geophys. Res. Lett., 35(13), L13815, doi:10.1029/2008GL033906, 2008b.

Lack, D. A., Moosmüller, H., McMeeking, G. R., Chakrabarty, R. K. and Baumgardner, D.: Characterizing elemental, equivalent black, and refractory black carbon aerosol particles: A review of techniques, their limitations and uncertainties, Anal. Bioanal. Chem., 406(1), 99–122, doi:10.1007/s00216-013-7402-3, 2014.

Laing, J. R., Jaffe, D. A. and Hee, J. R.: Physical and optical properties of aged biomass burning aerosol from wildfires in Siberia and the Western USA at the Mt. Bachelor Observatory, Atmos. Chem. Phys., 16(23), 15185–15197, doi:10.5194/acp-16-15185-2016, 2016.

Levenberg, K.: A method for the solution of certain non-linear problems in least squares, Q. Appl. Math., 2(2), 164–168, 1944.

Lewis, K., Arnott, W. P., Moosmüller, H. and Wold, C. E.: Strong spectral variation of biomass smoke light absorption and single scattering albedo observed with a novel dual-wavelength photoacoustic instrument, J. Geophys. Res. Atmos., 113(16), 1–14, doi:10.1029/2007JD009699, 2008.

Li, H., Lamb, K. D., Schwarz, J. P., Selimovic, V., Yokelson, R. J., McMeeking, G. R. and May, A. A.: Inter-comparison of black carbon measurement methods for simulated open biomass burning emissions, Atmos. Environ., 206, 156–169, doi:10.1016/j.atmosenv.2019.03.010, 2019.

Lim, S., Lee, M., Kim, S.-W. and Laj, P.: Sulfate alters aerosol absorption properties in East Asian outflow, Sci. Rep., 8(1), 5172, doi:10.1038/s41598-018-23021-1, 2018.

Liu, S., Aiken, A. C., Arata, C., Dubey, M. K., Stockwell, C. E., Yokelson, R. J., Stone, E. A., Jayarathne, T., Robinson, A. L., DeMott, P. J. and Kreidenweis, S. M.: Aerosol single scattering

albedo dependence on biomass combustion efficiency: Laboratory and field studies, Geophys. Res. Lett., 41(2), 742–748, doi:10.1002/2013GL058392, 2014.

McMeeking, G. R., Fortner, E., Onasch, T. B., Taylor, J. W., Flynn, M., Coe, H. and Kreidenweis, S. M.: Impacts of nonrefractory material on light absorption by aerosols emitted from biomass burning, J. Geophys. Res. Atmos., 119(21), 12,272-12,286, doi:10.1002/2014JD021750, 2014.

Moosmüller, H., Chakrabarty, R. K. and Arnott, W. P.: Aerosol light absorption and its measurement: A review, J. Quant. Spectrosc. Radiat. Transf., 110(11), 844–878, doi:10.1016/j.jqsrt.2009.02.035, 2009.

Moteki, N., Kondo, Y. and Nakamura, S.: Method to measure refractive indices of small nonspherical particles: Application to black carbon particles, J. Aerosol Sci., 41(5), 513–521, doi:10.1016/j.jaerosci.2010.02.013, 2010.

Müller, T., Henzing, J. S., de Leeuw, G., Wiedensohler, A., Alastuey, A., Angelov, H., Bizjak, M., Collaud Coen, M., Engström, J. E., Gruening, C., Hillamo, R., Hoffer, A., Imre, K., Ivanow, P., Jennings, G., Sun, J. Y., Kalivitis, N., Karlsson, H., Komppula, M., Laj, P., Li, S.-M., Lunder, C., Marinoni, A., Martins dos Santos, S., Moerman, M., Nowak, A., Ogren, J. A., Petzold, A., Pichon, J. M., Rodriquez, S., Sharma, S., Sheridan, P. J., Teinilä, K., Tuch, T., Viana, M., Virkkula, A., Weingartner, E., Wilhelm, R. and Wang, Y. Q.: Characterization and intercomparison of aerosol absorption photometers: result of two intercomparison workshops, Atmos. Meas. Tech., 4(2), 245–268, doi:10.5194/amt-4-245-2011, 2011a.

Müller, T., Laborde, M., Kassell, G. and Wiedensohler, A.: Design and performance of a three-wavelength LED-based total scatter and backscatter integrating nephelometer, Atmos. Meas. Tech., 4(6), 1291–1303, doi:10.5194/amt-4-1291-2011, 2011b.

Müller, T., Virkkula, A. and Ogren, J. A.: Constrained two-stream algorithm for calculating aerosol light absorption coefficient from the Particle Soot Absorption Photometer, Atmos. Meas. Tech., 7(12), 4049–4070, doi:10.5194/amt-7-4049-2014, 2014.

Nakayama, T., Kondo, Y., Moteki, N., Sahu, L. K., Kinase, T., Kita, K. and Matsumi, Y.: Size-dependent correction factors for absorption measurements using filter-based photometers: PSAP and COSMOS, J. Aerosol Sci., 41(4), 333–343, doi:10.1016/j.jaerosci.2010.01.004, 2010.

Nakayama, T., Suzuki, H., Kagamitani, S., Ikeda, Y., Uchiyama, A. and Matsumi, Y.: Characterization of a Three Wavelength Photoacoustic Soot Spectrometer (PASS-3) and a Photoacoustic Extinctiometer (PAX), J. Meteorol. Soc. Japan. Ser. II, 93(2), 285–308, doi:10.2151/jmsj.2015-016, 2015.

Ogren, J. A.: Comment on " Calibration and Intercomparison of Filter-Based Measurements of Visible Light Absorption by Aerosols ," Aerosol Sci. Technol., 44(December), 589–591, doi:10.1080/02786826.2010.482111, 2010.

Ogren, J. A., Wendell, J., Andrews, E. and Sheridan, P. J.: Continuous light absorption photometer for long-term studies, Atmos. Meas. Tech., 10(12), 4805–4818, doi:10.5194/amt-10-4805-2017, 2017.

Olson, M. R., Victoria Garcia, M., Robinson, M. A., Van Rooy, P., Dietenberger, M. A., Bergin, M. and Schauer, J. J.: Investigation of black and brown carbon multiple-wavelength-dependent

light absorption from biomass and fossil fuel combustion source emissions, J. Geophys. Res. Atmos., 120(13), 6682–6697, doi:10.1002/2014JD022970, 2015.

Rajesh, T. A. and Ramachandran, S.: Black carbon aerosol mass concentration, absorption and single scattering albedo from single and dual spot aethalometers: Radiative implications, J. Aerosol Sci., 119(January), 77–90, doi:10.1016/j.jaerosci.2018.02.001, 2018.

Saturno, J., Pöhlker, C., Massabò, D., Brito, J., Carbone, S., Cheng, Y., Chi, X., Ditas, F., Hrab De Angelis, I., Morán-Zuloaga, D., Pöhlker, M. L., Rizzo, L. V., Walter, D., Wang, Q., Artaxo, P., Prati, P. and Andreae, M. O.: Comparison of different Aethalometer correction schemes and a reference multi-wavelength absorption technique for ambient aerosol data, Atmos. Meas. Tech., 10(8), 2837–2850, doi:10.5194/amt-10-2837-2017, 2017.

Schmeisser, L., Andrews, E., Ogren, J. A., Sheridan, P., Jefferson, A., Sharma, S., Kim, J. E., Sherman, J. P., Sorribas, M., Kalapov, I., Arsov, T., Angelov, C., Mayol-Bracero, O. L., Labuschagne, C., Kim, S.-W., Hoffer, A., Lin, N.-H., Chia, H.-P., Bergin, M., Sun, J., Liu, P. and Wu, H.: Classifying aerosol type using in situ surface spectral aerosol optical properties, Atmos. Chem. Phys., 17(19), 12097–12120, doi:10.5194/acp-17-12097-2017, 2017.

Schmid, O., Artaxo, P., Arnott, W. P., Chand, D., Gatti, L. V., Frank, G. P., Hoffer, A., Schnaiter, M. and Andreae, M. O.: Spectral light absorption by ambient aerosols influenced by biomass burning in the Amazon Basin. I: Comparison and field calibration of absorption measurement techniques, Atmos. Chem. Phys., 6(11), 3443–3462, doi:10.5194/acp-6-3443-2006, 2006.

Schwarz, J. P., Spackman, J. R., Fahey, D. W., Gao, R. S., Lohmann, U., Stier, P., Watts, L. A., Thomson, D. S., Lack, D. A., Pfister, L., Mahoney, M. J., Baumgardner, D., Wilson, J. C. and Reeves, J. M.: Coatings and their enhancement of black carbon light absorption in the tropical atmosphere, J. Geophys. Res., 113(D3), D03203, doi:10.1029/2007JD009042, 2008.

Sedlacek, A. J.: DOE/SC-ARM-TR-156 Aethalometer^{TM} Instrument Handbook, DOE Office of Science Atmospheric Radiation Measurement (ARM) Program., 2016.

Selimovic, V., Yokelson, R. J., Warneke, C., Roberts, J. M., de Gouw, J., Reardon, J. and Griffith, D. W. T.: Aerosol optical properties and trace gas emissions by PAX and OP-FTIR for laboratory-simulated western US wildfires during FIREX, Atmos. Chem. Phys., 18(4), 2929–2948, doi:10.5194/acp-18-2929-2018, 2018.

Sheridan, P. J., Arnott, W. P., Ogren, J. A., Andrews, E., Atkinson, D. B., Covert, D. S., Moosmüller, H., Petzold, A., Schmid, B., Strawa, A. W., Varma, R. and Virkkula, A.: The Reno Aerosol Optics Study: An Evaluation of Aerosol Absorption Measurement Methods, Aerosol Sci. Technol., 39(1), 1–16, doi:10.1080/027868290901891, 2005.

Sherman, J. P., Sheridan, P. J., Ogren, J. A., Andrews, E., Hageman, D., Schmeisser, L., Jefferson, A. and Sharma, S.: A multi-year study of lower tropospheric aerosol variability and systematic relationships from four North American regions, Atmos. Chem. Phys., 15(21), 12487–12517, doi:10.5194/acp-15-12487-2015, 2015.

Springston, S. R.: DOE/SC-ARM-TR-176 Radiance Research Particle Soot/Absorption Photometer Instrument Handbook, DOE Office of Science Atmospheric Radiation Measurement (ARM) Program (United States)., 2016.

997 Subramanian, R., Roden, C. A., Boparai, P. and Bond, T. C.: Yellow Beads and Missing Particles:
998 Trouble Ahead for Filter-Based Absorption Measurements, Aerosol Sci. Technol., 41(6), 630–637,
999 doi:10.1080/02786820701344589, 2007.

1000 Vignati, E., Karl, M., Krol, M., Wilson, J., Stier, P. and Cavalli, F.: Sources of uncertainties in
1001 modelling black carbon at the global scale, Atmos. Chem. Phys., 10(6), 2595–2611,
1002 doi:10.5194/acp-10-2595-2010, 2010.

1003 Virkkula, A.: Correction of the Calibration of the 3-wavelength Particle Soot Absorption
1004 Photometer (3λ PSAP), Aerosol Sci. Technol., 44(8), 706–712,
1005 doi:10.1080/02786826.2010.482110, 2010.

1006 Virkkula, A., Ahlquist, N. C., Covert, D. S., Arnott, W. P., Sheridan, P. J., Quinn, P. K. and
1007 Coffman, D. J.: Modification, calibration and a field test of an instrument for measuring light
1008 absorption by particles, Aerosol Sci. Technol., 39(1), 68–83, doi:10.1080/027868290901963,
1009 2005.

1010 Virkkula, A., Mäkelä, T., Hillamo, R., Yli-Tuomi, T., Hirsikko, A., Hämeri, K. and Koponen, I.
1011 K.: A simple procedure for correcting loading effects of aethalometer data, J. Air Waste Manag.
1012 Assoc., 57(10), 1214–1222, doi:10.3155/1047-3289.57.10.1214, 2007.

1013 Virkkula, A., Chi, X., Ding, A., Shen, Y., Nie, W., Qi, X., Zheng, L., Huang, X., Xie, Y., Wang,
1014 J., Petäjä, T. and Kulmala, M.: On the interpretation of the loading correction of the aethalometer,
1015 Atmos. Meas. Tech., 8(10), 4415–4427, doi:10.5194/amt-8-4415-2015, 2015.

1016 Wang, X., Heald, C. L., Sedlacek, A. J., de Sá, S. S., Martin, S. T., Alexander, M. L., Watson, T.
1017 B., Aiken, A. C., Springston, S. R. and Artaxo, P.: Deriving brown carbon from multiwavelength
1018 absorption measurements: method and application to AERONET and Aethalometer observations,
1019 Atmos. Chem. Phys., 16(19), 12733–12752, doi:10.5194/acp-16-12733-2016, 2016.

1020 Weingartner, E., Saathoff, H., Schnaiter, M., Streit, N., Bitnar, B. and Baltensperger, U.:
1021 Absorption of light by soot particles: Determination of the absorption coefficient by means of
1022 aethalometers, J. Aerosol Sci., 34(10), 1445–1463, doi:10.1016/S0021-8502(03)00359-8, 2003.

1023